HHS Public Access

Author manuscript

Angiogenesis. Author manuscript; available in PMC 2022 May 01.

Published in final edited form as:

Angiogenesis. 2021 May ; 24(2): 327–344. doi:10.1007/s10456-020-09765-3.

Human endothelial colony-forming cells provide trophic support for pluripotent stem cell-derived cardiomyocytes via distinctively high expression of neuregulin-1

Xuechong Hong[1,2], **Nicholas Oh**[1,2], **Kai Wang**[1,2], **Joseph Neumeyer**[1], **Chin Nien Lee**[1,2], **Ruei-Zeng Lin**[1,2], **Breanna Piekarski**[1], **Sitaram Emani**[1,2], **Arin K. Greene**[3], **Ingeborg Friehs**[1,2], **Pedro J. del Nido**[1,2], **Juan M. Melero-Martin**[1,2,4]

[1]Department of Cardiac Surgery, Boston Children's Hospital, 300 Longwood Ave., Enders 349, Boston, MA 02115, USA

[2]Department of Surgery, Harvard Medical School, Boston, MA 02115, USA

[3]Department of Plastic and Oral Surgery, Boston Children's Hospital, Boston, MA 02115, USA

[4]Harvard Stem Cell Institute, Cambridge, MA 02138, USA

Abstract

The search for a source of endothelial cells (ECs) with translational therapeutic potential remains crucial in regenerative medicine. Human blood-derived endothelial colony-forming cells (ECFCs) represent a promising source of autologous ECs due to their robust capacity to form vascular networks in vivo and their easy accessibility from peripheral blood. However, whether ECFCs have distinct characteristics with translational value compared to other ECs remains unclear. Here, we show that vascular networks generated with human ECFCs exhibited robust paracrine support for human pluripotent stem cell-derived cardiomyocytes (iCMs), significantly improving protection against drug-induced cardiac injury and enhancing engraftment at ectopic (subcutaneous) and orthotopic (cardiac) sites. In contrast, iCM support was notably absent in grafts with vessels lined by mature-ECs. This differential trophic ability was due to a unique high constitutive expression of the cardioprotective growth factor neuregulin-1 (NRG1). ECFCs, but not mature-ECs, were capable of actively releasing NRG1, which, in turn, reduced apoptosis and increased the proliferation of iCMs via the PI3K/Akt signaling pathway. Transcriptional silencing of NRG1 abrogated these cardioprotective effects. Our study suggests that ECFCs are uniquely suited to support human iCMs, making these progenitor cells ideal for cardiovascular regenerative medicine.

Juan M. Melero-Martin, juan.meleromartin@childrens.harvard.edu.

Author contributions XH, R-ZL and JMM-M conceived and designed the project. XH, NO, KW, JN, C-NL, R-ZL, and JMM-M performed the experimental work. All authors discussed and analyzed the data and edited the results. BP, SE, and AKG, provided crucial material. XH and JMM-M wrote the manuscript.

Supplementary Information The online version contains supplementary material available at https://doi.org/10.1007/s10456-020-09765-3.

Conflict of interest The authors declare no competing financial interests.

Keywords

ECFC; Cardiomyocytes; Induced pluripotent stem cell; Neuregulin-1

Introduction

Coronary heart disease often leads to irreversible cardiomyocyte loss and heart failure, and it is one of the leading health burdens worldwide [1]. Current treatments are focused on limiting the initial ischemic injury and reducing successive remodeling progression. However, neither endogenous regeneration processes nor clinically available therapies can adequately compensate for the loss of cardiomyocytes. In recent years, human pluripotent stem cell-derived cardiomyocytes (iCMs) have emerged as an alternative autologous cell source with the potential for cardiac regeneration [2]. Indeed, cardiac tissue bioengineered with stem cell-derived cardiomyocytes represents a promising approach for cardiac repair. However, several hurdles hamper the clinical translation of engineered cardiac tissues, including reduced cardiomyocyte survival and retention as well as insufficient vascular integration with host vessels upon implantation [3].

The early establishment of a perfused microvascular network is crucial for the successful engraftment of bioengineered tissues, enabling adequate delivery of oxygen and nutrients and removing waste products from the grafts [4]. In addition, prompt vascularization is critical for the survival of the engrafted cardiomyocytes [5]. Although host blood vessels could be recruited from the tissues surrounding the implantation site [6, 7], consensus holds that vascularization of thick grafts requires a built-in vascular network that facilitates rapid and complete perfusion following implantation.

Over the last decade, efforts in cardiac tissue engineering have included bioengineering such vascular networks using various sources of human endothelial cells (ECs) [8–10]. Nevertheless, a critical question is the type of blood vessels and the nature of the endothelium that is more suitable for cardiomyocyte engraftment. Recent studies have demonstrated that the organotypic heterogeneity of the endothelium is associated with tissue-specific cellular interaction between ECs and parenchymal cells [11, 12]. This question is particularly important because the crosstalk between ECs and cardiomyocytes is crucial in regulating cardiomyocyte function [13, 14], and it remains fundamentally unexplored whether some types of clinically accessible ECs can recapitulate these cardiac tissue-specific interactions better than others.

Generally, there are two primary sources of autologous ECs corresponding to those originated from either progenitor cells or the lining of a mature vasculature (hereafter refer to as ECFCs and mature-ECs, respectively). ECFCs and mature-ECs are conceptually different (Fig. S1). On the one hand, ECFCs are differentiated, ex vivo, from circulating progenitor cells and thus have not previously been part of a functional blood vessel in vivo. In contrast, mature-ECs are derived from the lining of actual blood vessels and have previously functioned as ECs in vivo. Despite these differences, once in culture, ECFCs and mature-ECs exhibit a wide range of functional similarities, including a robust ability to form blood vessels following implantation in vivo [15–17]. Indeed, studies reporting functional

differences between ECFCs and mature-ECs are scarce, especially in the context of interactions between ECs and parenchymal cells.

Here, we investigate and compare the propensities of these two types of human ECs for supporting iCM engraftment. We used blood-derived ECFCs and white adipose tissue-derived ECs (wat-ECs) as representative of progenitor and mature-ECs, respectively. Both ECFCs and wat-ECs can be derived from their respective tissues of origin (blood and subcutaneous adipose tissue) via minimally invasive procedures, and thus, they are widely considered clinically accessible sources of autologous ECs [17–19].

We used various murine xenograft models to demonstrate that vascular networks formed by ECFCs support the engraftment of human iCMs significantly more robustly than those generated with mature-ECs, both at ectopic and orthotopic transplantation sites and in the presence or absence of myocardial injury. We show that this superior cardio-supportive ability of ECFCs is attributed to a distinct constitutive high expression of neuregulin-1 (NRG1), a growth factor associated with cardioprotective function. Our study suggests that ECFCs are uniquely suited to form microvascular niches that support human iCMs, making these progenitor cells ideal for cardiovascular regenerative medicine.

Results

Differential EC capacity to support cardiomyocytes in vivo

We used human cord blood-derived ECFCs and white adipose tissue-derived ECs (wat-ECs) as representative of ECFCs and mature-ECs respectively (Fig. S1). We first validated their endothelial phenotype. In culture, both populations of ECs displayed typical cobblestone-like morphology and expressed EC markers, including CD31 (*PECAM-1*), VE-Cadherin (*CDH5*), von Willebrand factor (*VWF*), VEGFR-2 (*KDR*), and eNOS (*NOS3*) (Fig. S2). Both ECFCs and mature-ECs were highly pure and showed uniform expression of CD31 (> 95%) as well as a negligible presence of either mesenchymal (CD90/THY1, PDGFRB) or hematopoietic (CD45) markers (Fig. S2). In vivo, upon subcutaneous implantation into immunodeficient mice, both ECFCs and mature-ECs displayed robust abilities to form vascular networks (Fig. S3), a critical validation of EC functionality that was consistent with previous characterizations of these cells [15–17].

To gain insights into the trophic capacity of both types of ECs on supporting cardiomyocytes, we first used a subcutaneous model to engraft human induced pluripotent stem cell (iPSC)-derived iCMs (see Fig. S4 and Video. S1 for iCM characterization) with ECFCs or mature-ECs into immunodeficient mice. This ectopic model allowed evaluating the interaction between iCMs and ECs without potentially compounding paracrine signals from the heart. We carried out a side-by-side comparison of grafts that contained iCMs in the presence of either ECFCs or mature-ECs (Fig. 1a). Macroscopic examination revealed that grafts that contained iCMs with ECs were thoroughly vascularized after 2 weeks (Fig. 1b). Histological (H&E) analysis confirmed a robust presence of perfused blood microvessels in grafts with either ECFCs or mature-ECs (Fig. 1b). In contrast, grafts with iCMs alone notably lacked perfused microvessels (Fig. 1c), confirming the importance of providing exogenous ECs to achieve adequate vascularization. In grafts seeded with ECs,

microvessels were primarily lined by human ECs, as confirmed by the expression of human-specific CD31 (hCD31) (Fig. 1d, e, Fig. S5A), and there were no statistical differences in human microvascular density between grafts with ECFCs or mature-ECs in vivo (Fig. 1d).

Next, we examined iCM abundance in each of the grafts - iCMs were identified by cTNT expression (Fig. 1e). The degree of iCM engraftment was similar among the different groups after 1 week. However, after 2 weeks, iCM engraftment was significantly more robust in the presence of vessels lined by ECFCs (average ~ 4% of the graft area occupied by cTNT + iCMs) than by mature-ECs (~ 1%) or in the absence of human vessels (~ 1%) (Fig. 1e, f). Moreover, within the grafts, there was a spatial correlation between the location of ECFCs (marked by hCD31+) and cTNT + iCMs ($R^2 = 0.81$) (Fig. 1g). In contrast, this spatial association was absent in grafts containing vessels lined by mature-ECs ($R^2 = 0.46$).

Previous studies have shown that vascularization in itself can improve the survival of cardiomyocytes in transplanted bioengineered cardiac patches [8]. However, we only found a significant enhancement in iCM engraftment in the presence of ECFCs. Indeed, iCM engraftment did not improve in grafts containing mature-ECs compared to grafts lacking human ECs (iCM alone group) (Fig. 1f). Although iCMs displayed similar patterns of the gap junction component connexin 43 (Cx-43) in both groups, we also found more organized iCM sarcomere structures with ECFCs than with mature-ECs (Fig. S5B, C), further suggesting differential effects in EC-iCM crosstalk.

The presence of ECFCs was associated with both a higher rate of iCM proliferation and a lower rate of apoptosis. Indeed, 1 week after implantation, the percentage of proliferating iCMs (i.e., Ki67+/cTNT + cells) was significantly higher in the presence of ECFCs (~ 12%) than with mature-ECs (~ 5.5%) or in the absence of human vessels (~ 5%) (Fig. 1h). Meanwhile, the percentage of apoptotic iCMs (i.e., TUNEL+/cTNT + cells) at 2 weeks was significantly lower in the presence of ECFCs (~ 4%) than with mature-ECs (~ 13%) or the absence of ECs (~ 10%) (Fig. 1i).

To determine whether ECFCs could also serve as trophic mediators supporting iCM engraftment on the heart, we examined two orthotopic models corresponding to implantation onto both uninjured and injured (i.e., permanent LAD ligation) myocardium in immunodeficient SCID mice (Fig. 2a). Implants containing iCMs alone served as control. After 2 weeks in vivo, all cardiac implants remained steadily attached to the hearts, and macroscopic examination suggested they were thoroughly vascularized (Fig. 2b). Histological (H&E) analysis revealed an abundant presence of perfused microvessels in all groups (Fig. 2c), with no statistical differences in microvascular density in both the uninjured and injured myocardial models, and in grafts containing either ECFCs or mature-ECs (Fig. 2c, d, f). In implants with exogenous ECs, hCD31 + microvessels were uniformity distributed throughout the grafts, whereas implants with only iCMs were solely vascularized by host vessels, which were preferentially located in the periphery.

Despite similarities in the degree of vascularization, however, there were significant differences in iCM engraftment. As occurred in the subcutaneous ectopic model, the engraftment of cTNT + iCMs at 2 weeks was significantly more robust in the presence of

ECFCs (average ~ 3% of the graft area occupied by cTNT + iCMs) than with mature-ECs (~ 1%) or in the absence of ECs (~ 1%) (Fig. 2d, e). These differences remained significant regardless of whether the myocardium was injured or uninjured. Also, the percentage of apoptotic iCMs (TUNEL+/cTNT + cells) was significantly lower with ECFCs (Fig. 2g). Nevertheless, it is important to note that despite the enhanced iCM engraftment with ECFCs, at 2 weeks there were no significant differences in infarct size among the different groups (Fig. 2h), which suggested that the differences observed between ECFCs and mature-ECs were likely independent of the severity of the infarct.

Together, the results from both the ectopic (subcutaneous) and orthotopic (cardiac) models indicated that the engraftment of human iCMs significantly improved with ECFCs. The presence of ECFCs, but not mature-ECs, distinctively supported iCMs, which preferentially located in the proximity of ECFC-lined vessels.

Human ECFCs distinctively exhibit high expression of NRG1

To gain insights into the mechanism by which ECFCs exerted distinct trophic support on iCMs, we first performed a transcriptome comparison between ECFCs and mature-ECs via RNA-Seq analysis. Globally, the vast majority of genes were not differentially expressed between the two EC populations (log2FC < 1; adjusted *P*-value > 0.05), which was expected considering their common endothelial identity (Fig. 3a; Fig. S6). Nonetheless, hundreds of differentially expressed genes were unique for each EC group (Fig. 3a), resulting in distinct patterns of variability and association, as confirmed by principal component analyses (Fig. 3b).

Mounting evidence indicates that the endothelium heterogeneity is associated with differential paracrine function and tissue-specific cellular crosstalk between ECs and parenchymal cells [11, 12]. This specialization includes the heart, where dynamic interactions between the endothelium and cardiomyocytes play essential roles in regulating cardiovascular development and homeostasis [13, 14]. In this crosstalk context, we analyzed differentially expressed genes that encode ligands with known effects on the activation of cellular receptors (gene ontology term GO:0048018, receptor-ligand activity; 490 genes) (Fig. 3d). We identified a cluster of 14 differentially enriched genes in ECFCs compared to mature-ECs (log2FC > 1, adjusted $P < 0.05$) (Fig. 3d). Among these genes, the expression of *NRG1*, a trophic growth factor associated with cardioprotective function, was of singular significance in ECFCs compared to mature-ECs (Fig. 3c–e).

We then examined the expression of *NRG1* at the mRNA level in multiple types of human ECs by quantitative PCR (qPCR). In addition to cb-ECFCs, we extended our analysis of ECFCs to ECFCs derived from human adult peripheral blood (ab-ECFCs). We also included two additional sources of human mature-ECs corresponding to myocardial microvasculature (myocard-ECs) and umbilical vein (HUVECs). We designed primers to recognize two of the most common *NRG1* isoforms: *NRG1* type I (*NRG1-I*) and type III (*NRG1-III*). Our analysis revealed that *NRG1-I* expression by both cord blood and adult ECFCs was significantly higher than by any of the mature-ECs examined (Fig. 4a). Indeed, the differences in *NRG1-I* expression between ECFCs and any of the mature-ECs was at least > eightfold higher. The high *NRG1-I* expression by ECFCs did not decrease with expansion

and passaging in vitro (Fig. S7A). In contrast, there were no significant differences in *NRG1-III* expression among all the groups (Fig. S7B). The distinct expression of NRG1 by both cb-ECFCs and ab-ECFCs was corroborated by immunofluorescence staining (Fig. 4b) and by western blot analysis (Fig. 4c), confirming that the differential expression was also present at the protein level.

NRG1 belongs to the neuregulin family of growth factors containing an extracellular epidermal growth factor (EGF)-like domain. Upon enzymatic cleavage, the EGF-like domain can bind to erythroblastic leukemia viral oncogene homolog (ErbB) receptors and stimulate a variety of cellular responses in a paracrine fashion [13, 20]. We assessed whether ECFCs actively released the extracellular domain of NRG1, a requirement for paracrine signaling potential. To this end, we generated conditioned media from both cb-ECFCs and ab-ECFCs and measured the levels of NRG1-I by ELISA. This analysis revealed that the concentration of NRG1 in media conditioned by ECFCs was significantly higher than in media conditioned by any of the mature-ECs tested (> 11-fold and > 14-fold higher for cb-ECFCs and ab-ECFCs, respectively) (Fig. 4d), thus confirming that ECFCs not only distinctively express NRG1, but also actively release its soluble bioactive form.

Next, we examined whether ECFCs maintained NRG1 expression upon engraftment in vivo. To this end, we used our subcutaneous vascular network forming model and carried out a side-by-side comparison of grafts that contained either ECFCs or mature-ECs in the absence of iCMs. After 7 days in vivo, both groups of grafts had become vascularized and contained an extensive network of perfused microvessels (Fig. 4e). These microvessels were primarily lined by human ECs, as confirmed by the expression of hCD31 (Fig. 4f). Importantly, immunofluorescence analysis confirmed the expression of NRG1 in lumens lined by ECFCs (Fig. 4f), and the proportion of NRG1 + human vessels was significantly higher in grafts containing ECFCs (~ 45%) compared to grafts with mature-ECs (~ 2%). We also examined the in vivo capacity of ECFCs to express NRG1 in the absence or presence of iCMs. In both cases, histological examination of the grafts corroborated an abundant presence of perfused microvessels that were primarily lined by hCD31 + ECs and distinctively expressed NRG1 in their lumens (Fig. 4g). We also analyzed mRNA in human ECs from explanted grafts and found that retrieved ECFCs displayed a significantly higher level of NRG1 expression than retrieved mature-ECs, irrespective of whether the grafts contained iCMs or not (Fig. 4h). (Please note that human MSCs, which are also used to support the engraftment of ECs in vivo, displayed minimal expression of NRG1 at the mRNA and protein levels (Fig. S7A, C)). Moreover, we measured the capacity to secrete NRG1 protein by explanted grafts using an ELISA kit and confirmed a significantly higher level of NRG1 secretion from grafts with ECFCs than with mature-ECs (Fig. 4i). Collectively, these data demonstrate that ECFCs continued to express and secrete NRG1 after their engraftment in vivo.

In summary, our data collectively indicated that ECFCs derived from both umbilical cord blood and adult peripheral blood distinctively exhibit high constitutive expression of NRG1 compared to various sources of mature-ECs. Moreover, we demonstrated that ECFCs actively release NRG1 into their extracellular environment. This differential NRG1 expression by ECFCs was evident at both the mRNA and the protein levels and maintained upon engraftment in vivo in the form of functional blood vessels.

ECFCs support iCMs via trophic NRG1 signaling

Previous studies have substantiated several beneficial cardiac-specific activities of NRG1 [13, 20]. Indeed, recombinant NRG1 protein can protect rodent primary cardiomyocytes against apoptosis, both in vitro and in vivo. Moreover, the EC-specific deletion of NRG1 in mice leads to impaired cardiac tolerance to ischemic injury [21]. In this context, we were particularly interested in examining whether the high NRG1 expression conferred ECFCs a distinct cardioprotective capability for human stem cell-derived cardiomyocytes.

First, we used a well-established model of in vitro cardiac injury that entails exposing cardiomyocytes to the chemotherapy drug doxorubicin (hereafter referred to as DOXO) [22]. We examined whether ECFCs can protect human iCMs against DOXO-induced injury through NRG1. We directly co-cultured iCMs with different ECs and exposed them to 1 μM of DOXO for 36 h. We then evaluated the severity of DNA damage in iCMs by measuring the accumulation of phosphorylated histone H2A.X (γ-H2A.X) that resulted from double-stranded DNA breaks (Fig. S8A). As expected, iCMs exposed to DOXO displayed a significant accumulation of γ-H2A.X compared with the control (vehicle-treated) group. However, the presence of ECFCs significantly reduced the accumulation of γ-H2A.X in DOXO-treated iCMs, suggesting protection against DNA damage (Fig. S8B). In contrast, when co-cultured with mature-ECs, the presence of γ-H2A.X in the nucleus of cTNT + iCMs remained abundant and significantly more prominent than with ECFCs (Fig. S8C). The expression of NRG1-I in ECFCs was not affected by the 36-h treatment with DOXO (Fig. S8D). These results suggested a distinct cardioprotective ability of ECFCs over mature-ECs.

Next, we examined whether the cardioprotective ability of ECFCs was due to secreted paracrine factors. To this end, we first incubated iCMs with conditioned medium from different ECs (EC-cm), followed by treatment with DOXO (2 μM) for 36 h (Fig. 5a). Examination of γ-H2A.X abundance in DOXO-treated iCMs revealed that ECFC-cm was distinctively protective compared to basal medium and mature-EC-cm (Fig. 5b, c), which was consistent with the results from the direct co-culture experiments (Fig. S8). We also examined whether the cardioprotective effect of ECFCs was due to NRG1. To this end, we used conditioned medium collected from ECFCs with siRNA-silenced *NRG1* (referred to as ECFC(siNRG1)-cm), which exhibited an approximately 70% reduction of NRG1-I expression (Fig. S9). This ECFC(siNRG1)-cm displayed a significantly attenuated protection against DOXO-induced DNA damage in iCMs (Fig. 5b, c). Similarly, the use of an inhibitor to ErbB receptors (AST1306) significantly diminished the cardioprotective effect of ECFC-cm (Fig. 5b, c), confirming that NRG1 in part mediated this outcome.

Beyond preventing DNA damage, we also examined the effect of ECFCs on the disruption of sarcomere structures and apoptosis in iCMs, both well-known consequences of DOXO exposure. We demonstrated that, in contrast to mature-EC-cm, pretreatment with ECFC-cm largely prevented myofilament disarray of the sarcomere structures in iCMs exposed to DOXO (2 μM) for 48 h (Fig. 5d). Moreover, this protection was significantly diminished in the presence of AST1306 (Fig. 5d), suggesting that the effect was mediated via NRG1-ErbB signaling. The effects on apoptosis were equally revealing. In the presence of ECFC-cm, the degree of caspase-3 activation in DOXO-treated iCMs was comparable to that found in

untreated iCMs and significantly lower than the activation produced by mature-EC-cm (Fig. 5e). Once again, the anti-apoptotic effect of ECFC-cm was abrogated by AST1306, confirming the role of NRG1-ErbB signaling (Fig. 5e). The effects on apoptosis were further confirmed via flow cytometry. In response to DOXO treatment, the percentage of both early (Annexin-V+/PI−) and late (Annexin-V+/PI+) apoptotic iCMs were significantly lower in the presence of ECFC-cm (Fig. S10).

Next, we analyzed the expression of NRG1 receptors ERBB2, ERBB3, and ERBB4 in iCMs at both the mRNA and protein levels (Fig. S11A, B). ERBB2 was more abundantly expressed in iCMs compared to ERBB3 and ERBB4 (Fig. S11A). The predominant expression of ERBB2 in iCMs is consistent with previous studies that have shown that ERBB2 plays a key role in regulating cardiomyocyte proliferation at embryonic/neonatal stages and promoting cardiomyocyte survival following ischemia injury [23–25]. In addition, studies have shown that ERBB2, but not ERBB4, is necessary for NRG1-induced proliferation in mouse neonatal cardiomyocyte [23]. We further confirmed the expression and activation (phosphorylation) of ERBB2 in iCMs. Indeed, iCMs treated with ECFC-cm upregulated phosphorylated ERBB2 (p-ERBB2) expression, but this activation was attenuated when treated with NRG1-knockdown ECFC-cm (Fig. S11C, D).

Previous studies have suggested that NRG1 mediates cardioprotection through the activation of the PI3K/Akt and MAPK/Erk signaling cascades [20]. Thus, we investigated whether the cardioprotective effect elicited by ECFCs was consistent with the activation of these signaling pathways. Immunoblotting analysis revealed that DOXO-treated iCMs that were pretreated with ECFC-cm displayed a reduced level of γ-H2A.X concurrently with enhanced activation of phosphorylated Akt (pAkt) (Fig. 5f). In contrast, mature-EC-cm failed to reduce γ-H2A.X and did not activate pAkt significantly. Meanwhile, the level of phosphorylated Erk1/2 showed no apparent difference among groups. Immunofluorescent staining confirmed a significant accumulation of pAkt within the nuclei of DOXO-treated iCMs in the presence of ECFC-cm, but not with mature-EC-cm (Fig. 5g). Moreover, the addition of AST1306 deterred the activation of pAkt by ECFC-cm, suggesting NRG1 mediation (Fig. 5g). Lastly, the activation of pAkt coincided with a significant increase in the number of proliferative Ki67 + iCMs in the presence of ECFC-cm, but not with mature-EC-cm; also, adding AST1306 abrogated this proliferative effect (Fig. 5h). Together, these results indicated that ECFCs protected iCMs against DOXO-induced damage through PI3K/Akt-mediated mechanisms, but not through MAPK/Erk signaling.

To confirm whether NRG1 signaling mediated the enhanced engraftment of iCMs in vivo, we examined grafts containing ECFCs after 2 weeks. Specifically, we compared grafts containing iCMs in the presence of either ECFCs in which NRG1 was silenced via lentivirus-delivered shRNA (referred to as shNRG1) or control ECFCs (scrambled shRNA; termed shCTR) (validation of shRNA silencing depicted in Fig. 6a and Fig. S9). Quantification of cTNT + iCM abundance within the grafts revealed that NRG1 expression in ECFCs was indeed mediating the enhanced engraftment – iCMs presence was significantly lower in the presence of ECFCs (shNRG1) (~ 1% of the graft area) than with control ECFCs (shCTR) (~ 2.7%) (Fig. 6b, c). Also, in the presence of ECFCs (shNRG1), there were both significantly less proliferative Ki67 + iCMs at 1 week (Fig. 6d) and more

TUNEL + iCMs at 2 weeks (Fig. 6e) compared to grafts with control ECFCs (shCTR). In summary, these results demonstrated an enhanced ability of ECFCs over mature-ECs to support iCM engraftment in vivo, which was, in part, due to their differential constitutive expression of NRG1.

Discussion

The search for alternative means of improving the engraftment and retention of cardiomyocytes remains crucial in cardiac regenerative medicine. Here, we report that the use of ECFCs could be instrumental to this end. We demonstrate that human ECFCs derived from both adult peripheral and umbilical cord blood distinctively express high constitutive levels of the cardioprotective growth factor NRG1 compared with mature-ECs. This differential NRG1 expression was evident at both the mRNA and the protein levels and maintained upon forming functional blood vessels in vivo. Moreover, ECFCs actively cleave and release NRG1, which in turn conferred paracrine protection to iCMs. We demonstrated constitutive ECFC-mediated cardioprotection in vitro (DOXO-induced cardiotoxicity) and in vivo (engraftment into immunodeficient mice). Cardioprotection by ECFCs was significantly superior to that produced by mature-ECs and was mediated by NRG1 via the activation of the PI3K/Akt signaling pathway in iCMs. In vivo, using ectopic (subcutaneous) and orthotopic (cardiac) xenografts, exogenous ECFCs, but not mature-ECs, significantly enhanced the engraftment of iCMs, an effect also regulated by NRG1.

The presence of ECs and the dynamic interactions between the cardiac endothelium and cardiomyocytes are crucial in regulating cardiac development and homeostasis [13]. Indeed, studies have shown that the removal of cardiac ECs produce significant detrimental effects on adjacent cardiomyocytes' function, suggesting that ECs play a critical role in regulating heart function [26, 27]. Previous studies established that ECs directly support cardiomyocytes through paracrine signaling, and several endothelial-derived cardioactive factors have been identified, including NRG1 [13, 20, 21]. During cardiac development, endocardial ECs release NRG1, which, in turn, activates ErbB receptors on cardiomyocytes to modulate ventricular trabeculation [28]. Postnatally, NRG1/ErbB signaling remains critical for cardiac adaptation to physiological (e.g., pregnancy and exercise) and pathological (e.g., cardiac ischemia/reperfusion) stresses [29–31]. From a translational standpoint, harnessing the paracrine potential of ECs to recapitulate the functional interdependency between cardiac ECs and cardiomyocytes could be critical for improving iCM engraftment. Nevertheless, the isolation of human cardiac-specific ECs for clinical use is not feasible, and thus alternative sources need to be considered.

Our study demonstrates that not all types of human ECs provide equal trophic support for iCMs. We found that only ECFCs, both from adult and cord blood, displayed cardiac-specific paracrine support via, in part, constitutive expression of NRG1. Transcriptional silencing of NRG1 and inhibition of ErbB receptor signaling abrogated the cardioprotective effect of ECFCs, confirming the role of NRG1. In contrast, the expression of NRG1 was negligible in several types of mature-ECs, including wat-ECs and HUVECs. This lack of NRG1 expression, however, did not preclude EC functionality. Indeed, mature-ECs displayed proper vasculogenic ability in vivo, consistent with previous studies that showed

revascularization of cardiac grafts with HUVECs [8, 10, 32]. The blood vessel-forming ability of mature-ECs was similar to that of ECFCs. However, the ability to support iCMs was notably different. Once the blood vessels were formed, only those lined by ECFCs exhibited paracrine protection of iCMs in the context of both drug-induced cardiotoxicity and engraftment in vivo. Notably, this protection was absent when mature-ECs lined the vessels. Nonetheless, it is important to note that our study only examined early iCM engraftment and not the long-term benefits to the heart. Previous studies have substantiated the efficacy of using iCMs as myocardial cell therapy [2, 33, 34]. Thus, further investigations are warranted to determine the long-term effects of transplanting ECFCs with iCMs on heart function.

Our findings are significant in understanding the crosstalk between human-specific ECs and cardiomyocytes. Previously, the interactions between ECs and cardiomyocytes have been studied for years, both during development and after myocardial injuries. However, most of these investigations were conducted in rodents, and studies that systematically address human-specific EC-cardiomyocytes interactions are lacking. One of the main challenges has been the absence of a dependable source of functional human cardiomyocytes. However, recently, the establishment of protocols to reliably derive iCMs from human iPSCs has enabled a more comprehensive examination of human cardiomyocyte behavior in response to injuries. For instance, in recent years, studies have demonstrated that human iCMs can recapitulate the cardiotoxicity produced by drugs like doxorubicin [35] and that iCMs can be used to develop human cardiac organoids that response to injury [36]. However, studies of human-specific iCM-EC interaction remained scarce [37]. Also, whether EC heterogeneity affects both the behavior of iCMs and the mechanisms of paracrine cardioprotection was unknown. Furthermore, the role of NRG1 and its effects on cardiomyocytes have primarily been established in mature cardiomyocytes, but not in iPSC-derived iCMs. Here, we confirmed that NRG1 has cardioprotective effects and provided new insights regarding NRG1 release from ECFCs but not from mature-ECs and how this can be leveraged to enhance the engraftment of human iCMs.

Our study indicates that, compared to mature-ECs, ECFCs are particularly well suited to serve as trophic mediators for iCMs. Previously, studies had only reported an increased abundance of circulating ECFCs in the early phase of acute myocardial infarction (MI) [38–40]. However, no direct functional relationship between ECFCs and cardiomyocytes had previously been established, and before our study, it was unknown whether ECFCs were particularly attuned to confer myocardial protection.

In the context of revascularizing bioengineered cardiac tissues, most investigations to date were conducted with mature-ECs. Studies have previously described that incorporating HUVECs into cardiac patches improves vascularization and, in turn, cardiomyocyte function [8, 10, 32]. However, whether HUVECs—or any other type of mature-ECs—can confer paracrine protection remained fundamentally unexplored. Also, from a translational viewpoint, HUVECs and other mature-ECs present limitations for widespread clinical use in an autologous setting. In contrast, our results suggest that ECFCs could be particularly well-suited for cardiac tissue engineering because they constitute an autologous source of human ECs with easy accessibility (blood) and exhibit a unique ability to protect cardiomyocytes

against stresses. Two other studies previously used human ECFCs to demonstrate inosculation and perfusion of pre-vascularized cardiac patches implanted in rats [41, 42]. However, those studies did not compare ECFC with mature-ECs nor examined cardioprotection, expression of NRG1, or paracrine interactions between ECFCs and cardiomyocytes.

Lastly, beyond cardioprotection, our study could have broad implications for the advancement of ECFC research. Over the last two decades, human ECFCs have been isolated and studied by multiple laboratories worldwide. Studies have collectively established a phenotypic signature for ECFCs that includes expression of common EC markers and a lack of hematopoietic and mesenchymal markers [18]. Functionally, there is consensus in that ECFCs must exhibit significant proliferative capacity and possess vascular network forming potential in vitro and in vivo [19, 43, 44]. However, all these phenotypical and functional characteristics are hardly exclusive of ECFCs and are generally shared by mature-ECs in culture. Thus, the identification of distinct specific markers or functions that distinguish ECFCs from mature-ECs remains elusive. Our study suggests that the constitutive expression of NRG1 could serve as a distinct surrogate marker for human ECFCs. Indeed, high NRG1 expression was evident in ECFCs from both adult and umbilical cord blood, but notably absent in mature-ECs from the umbilical cord, adipose, and, to some extent, myocardial tissues. Also, ECFCs stably maintained this high NRG1 expression over extensive expansion in culture. Thus, we suggest NRG1 could serve as a unique marker for ECFCs and propose that trophic cardioprotection as a distinctive functional characteristic of ECFCs over mature-ECs.

Moreover, over the years, it has been suggested that circulating ECFCs may originate from various human organs, including bone marrow [45], the endothelial lining of large blood vessels such as the aorta [46], placenta [47], and white adipose tissue [48]. However, it remains unclear whether ECFCs from all these different tissues are phenotypically and functionally similar. Future studies should examine these multiple sources of putative ECFCs in light of their NRG1 expression and paracrine potential to elucidate possible similarities with blood-derived ECFCs.

In summary, our study demonstrates that human ECFCs are unique compared to mature-ECs in that they distinctively exhibit high constitutive expression of NRG1, which, in turn, confers these cells a robust ability to protect cardiomyocytes against stresses. These novel insights into the distinct biological properties of ECFCs should result in more rational exploitation of their therapeutic potential.

Methods

Isolation and culture of human ECFCs and MSCs

Human ECFCs were isolated from umbilical cord blood (cb-ECFCs) or adult peripheral blood (ab-ECFCs) samples in accordance with an Institutional Review Board-approved protocol as previously described [17]. Blood samples were collected using heparinized tubes. ECFCs were isolated from the mononuclear cell (MNC) fractions from the blood samples after Ficoll-Paque density gradient centrifugation and purified using CD31-coated

magnetic beads. Cells were plated on fibronectin (10 μg/ml in PBS, Chemicon, Cat No. FC-010) coated plates in EC medium. Medium was changed every 2 days. ECFC colonies with cobblestone-like cell morphology were emerged in culture after 2–3 weeks. ECFCs were then cultured on 1% gelatin-coated plates using EC medium. All experiments were performed with ECFCs before passage 12.

Human MSCs were isolated from the white adipose tissue as previously described [43]. h-MSCs were cultured on uncoated plates using MSC-medium: MSCGM (Lonza, Cat No. PT-3001) supplemented with 10% FBS and 1 × GPS. All experiments were performed with MSCs before passage 12.

Isolation of human ECs from adipose and myocardium tissues

Endothelial cells were isolated from normal human subcutaneous white adipose tissue and ventricular myocardial tissue. All these human samples were deidentified and discarded tissues obtained during clinical-indicated procedures in accordance with Institutional Review Board-approved protocols. Tissues were minced and enzymatically (collagenase and dispase) digested for 2 h at 37 °C. Erythrocytes were lysed with RBC lysis buffer (New England Biolabs, Cat No. 420301). Wat-ECs and myocard-ECs were isolated by magnetic activated cell sorting (MACS) using h-CD31-coated magnetic beads (Dynabeads, Invitrogen, Cat No. 11155D). Isolated ECs were cultured on 1% gelatin-coated plates using EC medium: EGM-2 (except for hydrocortisone; PromoCell, Cat No. C22111) supplemented with 10% GenClone FBS (Genesee, Cat No. 25-514) and 1× glutamine-penicillin-streptomycin (GPS, ThermoFisher, Cat No. 10378106). All experiments were performed with ECs before passage 12.

Generation of human iPSCs and differentiation towards iCMs

Human induced pluripotent stem cells (h-iPSCs) were generated and cultured as previously described [49]. In brief, h-iPSCs were generated through non-integrating episomal overexpression of reprogramming factors OCT4, SOX2, KLF4, L-MYC, and LIN28 into human MSCs via electroporation. H-iPSCs were cultured on Matrigel (Corning, Cat No. 354277) coated plate in mTeSR1 medium (STEMCELL, Cat No. 85850) and passaged when reaching 80% confluency. Cardiac differentiation was induced using STEMdiff™ cardiomyocyte differentiation kit (STEMCELL, Cat No. 05010) according to the manufacturer's protocol. Following 8 days of differentiation, metabolic selection was performed with lactate medium composed of RPMI 1640 medium (no glucose, ThermoFisher, Cat No. 11879020) supplemented with 1% sodium DL-lactate solution (60%, Sigma, Cat No. L4263) and B27 (minus insulin, ThermoFisher, Cat No. A1895601). After 2 days of lactate selection, purified iCMs were maintained in STEMdiff™ cardiomyocyte maintenance medium.

Animal care

Six-week-old athymic nude (nu/nu) mice and NOD/SCID mice were purchased from The Jackson Laboratory (Boston, MA). Mice were housed in compliance with Boston Children's Hospital guidelines, and all animal-related protocols were approved by the Institutional Animal Care and Use Committee.

Ectopic subcutaneous engraftment of iCMs

Subcutaneous engraftment of cardiomyocytes was evaluated in nude mice using human iCM. Human iCMs alone (1×10^6 per mouse) or iCMs in combination with ECs (cb-ECFCs or wat-ECs) and MSCs (2.2×10^6 total per mouse; cell proportion: iCMs:ECs:MSCs = 1:0.8:0.4) were mixed with 200 μL of pH neutral hydrogel solution composed of 3 mg/mL of bovine collagen I (Trevigen, Cat No. 3442-050-01), 3 mg/mL of fibrinogen, 1 μg/mL of FGF2 (Peprotech, Cat No. 100-18B) and 1 μg/mL EPO (ProSpec, Cat No. CYT-201). Thrombin (50 μL of 10 U/mL; Sigma, Cat No. T4648) was then subcutaneously injected on the dorsal lateral flank of the animal. Next, the cell-hydrogel mixture (200 μL) was injected into the same site. All experiments were carried out in at least 5 mice. Explants were harvested after 1 week and 2 weeks for analysis.

Retrieval of hCD31 + cells from subcutaneous grafts

Explants were harvested, minced and enzymatically (collagenase and dispase) digested for 2 h at 37 °C. hCD31 + ECs were isolated by magnetic activated cell sorting (MACS) using hCD31-coated magnetic beads (Dynabeads, Invitrogen, Cat No. 11155D).

Orthotopic engraftment of iCMs on the uninjured myocardium

Orthotopic engraftment of cardiomyocytes was evaluated in NOD/SCID mice using human iCM in a cardiac patch implanted on top of the uninjured myocardium. Cardiac patched were constructed with human iCMs alone (5×10^5 per patch) or iCMs in combination with ECs (cb-ECFCs or wat-ECs) and MSCs (1.1×10^6 total per patch; cell proportion: iCMs:ECs:MSCs = 1:0.8:0.4) were mixed with 75 μL of pH neutral hydrogel solution composed of 3 mg/mL of bovine collagen I (Trevigen, Cat No. 3442-050-01), 3 mg/mL of fibrinogen, 1 μg/mL of FGF2 (Peprotech, Cat No. 100-18B) and 1 μg/mL EPO (ProSpec, Cat No. CYT-201). All cell-laden cardiac patches were polymerized by incubation at 37 °C for 30 min prior to their implantation in mice. For cardiac patch implantation, mice were anesthetized, intubated with 20-G catheter, and mechanically ventilated. Next, the anterior surface of the heart was exposed by a left thoracotomy and the pericardium was partially removed. The cardiac patch was placed onto the left ventricle of the heart and attached using two 8-0 polyprophylene sutures. All experiments were carried out in at least 3 mice. The hearts containing the cardiac patches were harvested after 2 weeks for analysis. Hearts were short-axis-sectioned through the patch.

Orthotopic engraftment of iCMs on the infarcted myocardium

Cardiac patch was constructed the same way as described above. NOD/SCID mice underwent left thoracotomy and the anterior surface of the heart was exposed. The pericardium was partially removed, and the heart was scuffed slightly with a cotton swab. An 8-0 nylon suture was used to ligate the left anterior descending artery (LAD) to create a myocardial infarction. Criteria for occlusion success was an acute color change in the left ventricular wall (red to pale). Afterwards, the cardiac patch was placed directly over the site of injury and sutured in place using an 8-0 suture. All experiments were carried out in at least 3 mice. The hearts containing the cardiac patches were harvested after 2 weeks for analysis. Hearts were short-axis-sectioned through the infarcted area and patch.

Histology and immunofluorescence staining

Tissue samples were fixed in 10% buffered formalin, embedded in paraffin and sectioned (7 μm thick). Microvessel density was reported as the average number of erythrocyte-filled vessels (vessels/mm^2) in H&E-stained sections from the middle of the samples as previously described [50]. Infarct area was assessed with Masson's Trichrome staining. Infarcted area was quantified and normalized to the left ventricular area in each section by Image J. For immunostainings, sections were deparaffinized and rehydrated through sequential immersion in xylene, 100%, 90%, 80% and 50% ethanol. Antigen retrieval was carried out by heating the sections in Tris-EDTA buffer. Sections were then blocked for 30 min in 5% blocking serum followed by incubation with primary antibodies overnight at 4 °C. Human-specific anti-CD31 antibody and the lectin *Ulex Europaeus Agglutinin* I (UEA-I) were used to stain human blood vessels. Fluorescent secondary antibodies were applied to the sections for 1 h at room temperature followed by nuclei counterstaining with DAPI. Finally, sections were mounted with fluorescent mounting medium (Dako). iCM engraftment area was calculated by cardiac Troponin T positive area divided by total grafting area measured by Image J. Spatial correlations between the location of ECs and iCMs were estimated by measuring the fluorescent intensity of hCD31 and cTNT in randomly selected fields within the grafts and then calculating the Pearson correlation coefficient of hCD31 and cTNT intensities.

RNA-sequencing (RNA-Seq) analysis

RNA-Seq was performed on cb-ECFCs, wat-ECs and MSC and was used to compare the differences between progenitor- and mature-ECs. Each cell type consisted of 3 biological replicates. Total RNA was extracted using Rneasy Mini Kit (Qiagen) following the manufacturer's protocol. RNA quantity and quality were checked with nanodrop and Agilent Bioanalyzer instrument. Libraries were prepared and sequenced by GENEWIZ (NJ, USA). Library preparation involved mRNA enrichment and fragmentation, chemical fragmentation, first and second strand cDNA synthesis, end repair and 5' phosphorylation, Da-tailing, adaptor ligation, and PCR enrichment. Libraries were then sequenced using Illumina HiSeq2500 platform (Illumina, CA) using 2 × 150 paired end configuration. Raw sequencing data (FASTQ hies) was examined for library generation and sequencing using FastQC (Babraham Institute) to ensure data quality. Reads were aligned to UCSC hg38 genome using the STAR aligner [51]. Alignments were checked for evenness of coverage, rRNA content, genomic context of alignments, complexity, and other quality checks using a combination of FastQC and Qualimap [52]. The expression of the transcripts was quantified against the Ensembl release GRCh38 transcriptome annotation using Salmon. These transcript abundances were then imported into R (version 3.5.1) and aggregated to the gene level with tximport. Differential expression at the gene level was called with DESeq2 [53]. Pairwise differential expression analysis between groups was performed using Wald significance test. P values were corrected for multiple hypothesis testing with the Benjamini-Hochberg false-discovery rate procedure (adjusted P value). Genes with adjusted P value < 0.05 were considered significantly different. PCA analysis was performed on DESeq2 normalized, rlog variance stabilized reads. All samples comparison was performed using Likelihood Ratio Test (LRT). Heat maps of differential expressed genes and enriched gene sets were generated with pheatmap package. Volcano plots of enriched gene sets were

generated with ggplot2 package. The RNA-Seq datasets are deposited online with SRA accession number: PRJNA509218.

Immunofluorescence staining

Cells were cultured in 4-well LAB-TEK chamber slides until confluency. Cells were fixed in 4% paraformaldehyde (PFA) for 10 min, permeabilized with 0.1% Triton X-100 while staining for intracellular protein, and then blocked for 30 min in 5% blocking serum. Samples were then incubated with primary antibodies diluted in 5% blocking serum overnight at 4 °C. After washing 3 times with PBS, samples were incubated with fluorescent secondary antibodies for 45 min at room temperature. Next, samples were washed 3 times with PBS and stained with 0.5 μg/mL DAPI for 5 min. Slides were mounted with DAKO fluorescence mounting medium (Agilent, Cat No. S302380-2). Antibodies are detailed in Table S2.

Flow cytometry

Cells were dissociated into single-cell suspensions using TrypLE and washed with PBS supplemented with 1% BSA and 0.2 mM EDTA. For iCMs, cells were fixed with 1% PFA for 10 min and permeabilized with 0.1% saponin for 10 min. In indicated experiments, flow cytometry antibodies (Table S2) and corresponding isotype-matched IgG antibodies were applied to stain the cells for 20 min followed by PBS wash for 3 times. A Guava easyCyte 6HT/2L flow cytometer (Millipore Corporation, Billerica, MA) was used to perform the analysis. Data was collected and analyzed with FlowJo software (Tree Star Inc., Ashland, OR).

Quantitative real-time PCR

Total RNA extraction from cultured cells was performed with RNeasy mini kit (Qiagen, Cat No. 74106) according to the protocol provided by the manufacturer. RNA concentration was measured with Nanodrop and the purity of the RNA was assessed by the ratio of absorbance at 260 nm and 280 nm. High-capacity cDNA reverse transcription kit (ThermoFischer, Cat No. 4368814) was applied as specified by the manufacturer to synthesize cDNA from total RNA. Quantitative real-time PCR was performed to detect and quantify gene expression using SYBR Green Master Mix (ThermoFisher, Cat No. A25776). A StepOnePlus real-time PCR system thermocycler (Applied Biosystems) was used to carry out the PCR reaction. Threshold cycle numbers (Ct) were measured in the exponential phase for all samples. Fold change was calculated as the relative fold difference of Ct value of target gene against GAPDH housekeeping gene. Sequences of primers for real-time PCR are listed in Table S3.

Western blot

Harvested cells were lysed with RIPA Lysis Buffer (Thermo Fisher, Cat No. 89901) supplemented with protease inhibitor and phosphatase inhibitor. The protein concentration was measured using Pierce 660 nm Protein Assay Reagent (Thermo Fisher, Cat No. 1861426) and a Bio-Rad Smart-SpecTM 3000 spectrophotometer. 40 μg of protein lysate was applied to 4–15% Mini-PROTEAN TGX precast protein Gel (Bio-Rad, Cat No. 4561084) with electrophoresis and then transferred to a nitrocellulose membrane, followed

by a standard western blotting procedure. The bound primary antibodies were detected using the Horseradish Peroxidase (HRP)-conjugated secondary antibodies and the Enhanced Chemiluminescent (ECL) detection system (GE Health, Cat No. 28906836). Primary and secondary antibodies are detailed in Table S2.

ELISA analysis

Cells were seeded at the density of 1×10^6 cells per 10-cm petri-dish in EC medium overnight. Medium was changed to 6 mL EBM-2 basal medium supplemented with 2% FBS the following day. Medium was collected after 48 h incubation and cell number was counted at the time of medium collection. Protease inhibitor was added into the medium. Medium was concentrated tenfold using 10K Ultracel (Millipore, Cat No. UFC901024) and the medium volume after concentration was recorded. Explants from the in vivo subcutaneous engraftment model were harvested, cut into smaller pieces and left in 500 μl EBM-2 basal medium supplemented with 2% FBS for 24 h. NRG1 released into the culture medium was measured using human NRGl-beta 1 DuoSet ELISA kit (R&D systems, Cat No. DY377-05). The quantity of NRG1 was calculated as the ratio of NRG1 in the medium normalized to the concentration ratio and the cell number.

In vivo vascular network-forming assay

Vascular network-forming assay was performed in vivo using our subcutaneous xenograft model in nude mice, as previously described [50]. Briefly, human ECs (cb-ECFCs or wat-ECs) and MSCs (2×10^6 total per mouse; EC:MSC = 2:1) were mixed with 200 μL of pH neutral hydrogel solution composed of 3 mg/mL of bovine collagen I (Trevigen, Cat No. 3442-050-01), 3 mg/mL of fibrinogen, 1 μg/mL of FGF2 (Peprotech, Cat No. 100-18B) and 1 μg/mL EPO (ProSpec, Cat No. CYT-201). Thrombin (50 μL of 10 U/mL; Sigma, Cat No. T4648) was then subcutaneously injected on the dorsal lateral flank of the animal. Next, the cell-hydrogel mixture (200 μL) was injected into the same site. All experiments were carried out in at least 3 mice. Explants were harvested after 1 week and 2 weeks for analysis.

NRG1 knockdown via siRNA

Human NRG1 Silencer® Select Pre-designed siRNA (Cat No. 4392420) and Silencer® Select Negative Control #1 siRNA (Cat No. 4390843) were purchased from Life Technologies. cb-ECFCs were transfected with 20 μL (per 10^6 cells) of 10 μM siRNA using Lipofectamine 3000 (ThermoFisher, Cat No. L3000008) according to the manufacturer's protocol. Cells were used in indicated experiments 48 h after transfection.

Doxorubicin treatment of iCMs

iCMs at differentiation day 14 were thoroughly dissociated, filtered through a 100 μM cell strainer and counted. iCMs were reseeded on Matrigel-coated plates at a density of 4×10^5 cells per well in 12-well plates and 5×10^4 cells per well in 96-well black-sided plates in STEMdiff™ cardiomyocyte maintenance medium. When iCMs reached confluency, 2 μM doxorubicin hydrochloride (MedChem Express, Cat No. HY-15142) was added to the culture medium for 24 h to 72 h. For iCMs and ECs co-culture experiments, iCMs and ECs were seeded on Matrigel coated plates at a ratio of 1:1 and cultured in medium composed of

50% EC medium and 50% cardiomyocyte maintenance medium until confluency. 1 μM doxorubicin was added to the culture medium for 36 h.

Conditioned medium generation and treatment of iCMs

Cells were seeded at the density of 1×10^6 cells per 10-cm petri-dish in EC medium overnight. Medium was changed to 6 mL EBM-2 basal medium supplemented with 2% FBS the following day. Conditioned medium was collected after 48 h incubation and filtered through 0.2 μM filters. Conditioned medium was then concentrated tenfold using 10K Ultracel. For indicated experiments, conditioned medium was mixed with cardiomyocyte maintenance medium to a 1:1 ratio and used to culture iCMs for 12 h before doxorubicin treatment.

DNA damage evaluation with γ-H2A.X

Persistent accumulation of γ-H2A.X is an indication of double strand DNA breaks and DNA damage [54]. γ-H2A.X is a widely used marker to evaluate DNA damage induced by doxorubicin [35, 55]. After doxorubicin treatment, iCMs seeded in 96-well black-sided plates were co-stained for cardiac Troponin T (cTNT) and γ-H2A.X by immunofluorescence. Pictures were taken at randomly selected fields and processed by Image J. Quantification of γ-H2A.X was calculated as the mean intensity of γ-H2A.X signal within the nuclei of cTNT + cells.

Caspase 3/7 activity assay

Caspase 3/7 activity was evaluated using NucView® 488 Caspase-3 Substrate (Biotium, Cat No. 10402) according to the protocol provided by the manufacturer. iCMs treated with 2 μM doxorubicin for 72 h with or without EC-conditioned medium were subjected to 5 μM Caspase-3 substrate for 30 min at room temperature. Nuclei were counterstained with Hoechst 33342 dye (ThermoFisher, Cat No. 62249).

Annexin V and PI staining

Cell apoptosis was measured using an eBioscience Annexin V-APC apoptosis detection kit (ThermoFisher, Cat No. 88-8007-72) and propidium iodide staining solution (ThermoFisher, Cat No. 00-6990-50) according to the protocol provided by the manufacturer. iCMs treated with 2 μM doxorubicin for 72 h with or without ECFC-conditioned medium were subjected to the staining and measured with flow cytometry.

NRG1 knockdown via short hairpin RNA (shRNA)

Human NRG1 shRNA lentiviral particles (Cat No. sc-37210-V) and control shRNA lentiviral particles (Cat No. sc-108080) were purchased from Santa Cruz. cb-ECFCs were infected with lentiviral particles with a MOI of 2 using polybrene (Santa Cruz, Cat No. sc-134220). Stable clones were selected via Puromycin dihydrochloride (Sigma, Cat No. P8833) selection.

Microscopy

Images were taken by the Axio Observer Z1 inverted microscope (Carl Zeiss) and AxioVision Rel. 4.8 software. Fluorescent images were taken with an ApoTome.2 Optical sectioning system (Carl Zeiss) and 10×, 20× or 40× objective lens. Non-fluorescent images were taken with an AxioCam MRc5 camera using a 10× or 20× objective lens.

Statistical analyses

All statistical analyses were performed using the Graph-Pad Prism v.5 software (GraphPad Software Inc.). Unless otherwise stated, data were expressed as mean ± standard deviation of the mean (s.d.). Comparisons between multiple groups were performed by ANOVA followed by Bonferro-ni's post-test analysis. Unpaired two-tailed Student's *t*-tests was used for comparisons between two groups. Samples size, including number of mice per group, was chosen to ensure adequate power and were based on historical laboratory data. No exclusion criteria were applied for all analyses. A value of $P < 0.05$ was considered to be statistically significant.

Supplementary Material

Refer to Web version on PubMed Central for supplementary material.

Acknowledgements

We thank Dr. Joyce Bischoff for providing some samples of adult peripheral blood-derived ECFCs. This work was supported by grants from the National Institutes of Health (R01AR069038 and R01HL128452 to J.M.M.-M.).

Data availability

The authors declare that all data supporting the findings of this study are available in the paper and its Supplementary Information.

References

1. Virani SS, Alonso A, Benjamin EJ, Bittencourt MS, Callaway CW, Carson AP, Chamberlain AM, Chang AR, Cheng S, Delling FN, Djousse L, Elkind MSV, Ferguson JF, Fornage M, Khan SS, Kissela BM, Knutson KL, Kwan TW, Lackland DT, Lewis TT, Lichtman JH, Longenecker CT, Loop MS, Lutsey PL, Martin SS, Matsushita K, Moran AE, Mussolino ME, Perak AM, Rosamond WD, Roth GA, Sampson UKA, Satou GM, Schroeder EB, Shah SH, Shay CM, Spartano NL, Stokes A, Tirschwell DL, VanWag-ner LB, Tsao CW, American Heart Association Council on E, Prevention Statistics C, Stroke Statistics S (2020) Heart disease and stroke statistics-2020 update: a report From the American Heart Association. Circulation 141(9):e139–e596. 10.1161/CIR.0000000000000757 [PubMed: 31992061]
2. Menasche P (2018) Cell therapy trials for heart regeneration—lessons learned and future directions. Nat Rev Cardiol 15(11):659–671. 10.1038/s41569-018-0013-0 [PubMed: 29743563]
3. Zhang J, Zhu W, Radisic M, Vunjak-Novakovic G (2018) Can we engineer a human cardiac patch for therapy? Circ Res 123(2):244–265. 10.1161/CIRCRESAHA.118.311213 [PubMed: 29976691]
4. Atala A, Kasper FK, Mikos AG (2012) Engineering complex tissues. Sci Transl Med 4(160):160rv112. 10.1126/scitranslmed.3004890
5. Ogle BM, Bursac N, Domian I, Huang NF, Menasche P, Murry CE, Pruitt B, Radisic M, Wu JC, Wu SM, Zhang J, Zimmermann WH, Vunjak-Novakovic G (2016) Distilling complexity to advance cardiac tissue engineering. Sci Transl Med 8(342):342ps313. 10.1126/scitranslmed.aad2304

6. Li X, Tjwa M, Moons L, Fons P, Noel A, Ny A, Zhou JM, Lennartsson J, Li H, Luttun A, Ponten A, Devy L, Bouche A, Oh H, Manderveld A, Blacher S, Communi D, Savi P, Bono F, Dewerchin M, Foidart JM, Autiero M, Herbert JM, Collen D, Heldin CH, Eriksson U, Carmeliet P (2005) Revascularization of ischemic tissues by PDGF-CC via effects on endothelial cells and their progenitors. J Clin Invest 115(1):118–127. 10.1172/JCI19189 [PubMed: 15630451]

7. Isner JM, Asahara T (1999) Angiogenesis and vasculogenesis as therapeutic strategies for postnatal neovascularization. J Clin Invest 103(9):1231–1236. 10.1172/JCI6889 [PubMed: 10225965]

8. Stevens KR, Kreutziger KL, Dupras SK, Korte FS, Regnier M, Muskheli V, Nourse MB, Bendixen K, Reinecke H, Murry CE (2009) Physiological function and transplantation of scaffold-free and vascularized human cardiac muscle tissue. Proc Natl Acad Sci USA 106(39):16568–16573. 10.1073/pnas.0908381106 [PubMed: 19805339]

9. Caspi O, Lesman A, Basevitch Y, Gepstein A, Arbel G, Habib IH, Gepstein L, Levenberg S (2007) Tissue engineering of vascularized cardiac muscle from human embryonic stem cells. Circ Res 100(2):263–272. 10.1161/01.RES.0000257776.05673.ff [PubMed: 17218605]

10. Tulloch NL, Muskheli V, Razumova MV, Korte FS, Regnier M, Hauch KD, Pabon L, Reinecke H, Murry CE (2011) Growth of engineered human myocardium with mechanical loading and vascular coculture. Circ Res 109(1):47–59. 10.1161/CIRCRESAHA.110.237206 [PubMed: 21597009]

11. Nolan DJ, Ginsberg M, Israely E, Palikuqi B, Poulos MG, James D, Ding BS, Schachterle W, Liu Y, Rosenwaks Z, Butler JM, Xiang J, Rafii A, Shido K, Rabbany SY, Elemento O, Rafii S (2013) Molecular signatures of tissue-specific microvascular endothelial cell heterogeneity in organ maintenance and regeneration. Dev Cell 26(2):204–219. 10.1016/j.devcel.2013.06.017 [PubMed: 23871589]

12. Marcu R, Choi YJ, Xue J, Fortin CL, Wang Y, Nagao RJ, Xu J, MacDonald JW, Bammler TK, Murry CE, Muczynski K, Stevens KR, Himmelfarb J, Schwartz SM, Zheng Y (2018) Human organspecific endothelial cell heterogeneity iScience 4:20–35. 10.1016/j.isci.2018.05.003

13. Parodi EM, Kuhn B (2014) Signalling between microvascular endothelium and cardiomyocytes through neuregulin. Cardiovasc Res 102(2):194–204. 10.1093/cvr/cvu021 [PubMed: 24477642]

14. Lim SL, Lam CS, Segers VF, Brutsaert DL, De Keulenaer GW (2015) Cardiac endothelium-myocyte interaction: clinical opportunities for new heart failure therapies regardless of ejection fraction. Eur Heart J 36(31):2050–2060. 10.1093/eurheartj/ehv132 [PubMed: 25911648]

15. Lin RZ, Lee CN, Moreno-Luna R, Neumeyer J, Piekarski B, Zhou P, Moses MA, Sachdev M, Pu WT, Emani S, Melero-Martin JM (2017) Host non-inflammatory neutrophils mediate the engraftment of bioengineered vascular networks. Nat Biomed Eng. 10.1038/s41551-017-0081

16. Melero-Martin JM, De Obaldia ME, Kang SY, Khan ZA, Yuan L, Oettgen P, Bischoff J (2008) Engineering robust and functional vascular networks in vivo with human adult and cord bloodderived progenitor cells. Circ Res 103(2):194–202. 10.1161/CIRCRESAHA.108.178590 [PubMed: 18556575]

17. Lin RZ, Moreno-Luna R, Li D, Jaminet SC, Greene AK, Melero-Martin JM (2014) Human endothelial colony-forming cells serve as trophic mediators for mesenchymal stem cell engraftment via paracrine signaling. Proc Natl Acad Sci USA 111(28):10137–10142. 10.1073/pnas.1405388111 [PubMed: 24982174]

18. Medina RJ, Barber CL, Sabatier F, Dignat-George F, Melero-Martin JM, Khosrotehrani K, Ohneda O, Randi AM, Chan JKY, Yamaguchi T, Van Hinsbergh VWM, Yoder MC, Stitt AW (2017) Endothelial progenitors: a consensus statement on nomenclature. Stem Cells Transl Med 6(5):1316–1320. 10.1002/sctm.16-0360 [PubMed: 28296182]

19. Nowak-Sliwinska P, Alitalo K, Allen E, Anisimov A, Aplin AC, Auerbach R, Augustin HG, Bates DO, van Beijnum JR, Bender RHF, Bergers G, Bikfalvi A, Bischoff J, Bock BC, Brooks PC, Bussolino F, Cakir B, Carmeliet P, Castranova D, Cimpean AM, Cleaver O, Coukos G, Davis GE, De Palma M, Dimberg A, Dings RPM, Djonov V, Dudley AC, Dufton NP, Fendt SM, Ferrara N, Fruttiger M, Fukumura D, Ghesquiere B, Gong Y, Griffin RJ, Harris AL, Hughes CCW, Hultgren NW, Iruela-Arispe ML, Irving M, Jain RK, Kalluri R, Kalucka J, Kerbel RS, Kitajewski J, Klaassen I, Kleinmann HK, Koolwijk P, Kuczynski E, Kwak BR, Marien K, Melero-Martin JM, Munn LL, Nicosia RF, Noel A, Nurro J, Olsson AK, Petrova TV, Pietras K, Pili R, Pollard JW, Post MJ, Quax PHA, Rabinovich GA, Raica M, Randi AM, Ribatti D, Ruegg C, Schlingemann RO, Schulte-Merker S, Smith LEH, Song JW, Stacker SA, Stalin J, Stratman AN, Van devan

Hinsbergh VM, Vermeulen VWM, Waltenberger PB, Weinstein J, Xin BM, Yetkin-Arik H, Yla-Herttuala B, Yoder S, Griffioen MC (2018) Consensus guidelines for the use and interpretation of angiogenesis assays. Angiogenesis 21(3):425–532. 10.1007/s10456-018-9613-x [PubMed: 29766399]

20. Odiete O, Hill MF, Sawyer DB (2012) Neuregulin in cardiovascular development and disease. Circ Res 111(10):1376–1385. 10.1161/CIRCRESAHA.112.267286 [PubMed: 23104879]
21. Hedhli N, Huang Q, Kalinowski A, Palmeri M, Hu X, Russell RR, Russell KS (2011) Endothelium-derived neuregulin protects the heart against ischemic injury. Circulation 123(20):2254–2262. 10.1161/CIRCULATIONAHA.110.991125 [PubMed: 21555713]
22. Gintant G, Burridge P, Gepstein L, Harding S, Herron T, Hong C, Jalife J, Wu JC (2019) Use of human induced pluripotent stem cell-derived cardiomyocytes in preclinical cancer drug cardiotoxicity testing: a scientific statement from the American Heart Association. Circ Res 125(10):e75–e92. 10.1161/RES.0000000000000291 [PubMed: 31533542]
23. D'Uva G, Aharonov A, Lauriola M, Kain D, Yahalom-Ronen Y, Carvalho S, Weisinger K, Bassat E, Rajchman D, Yifa O, Lysenko M, Konfino T, Hegesh J, Brenner O, Neeman M, Yarden Y, Leor J, Sarig R, Harvey RP, Tzahor E (2015) ERBB2 triggers mammalian heart regeneration by promoting cardiomyocyte dedifferentiation and proliferation. Nat Cell Biol 17(5):627–638. 10.1038/ncb3149 [PubMed: 25848746]
24. Aharonov A, Shakked A, Umansky KB, Savidor A, Genzelinakh A, Kain D, Lendengolts D, Revach OY, Morikawa Y, Dong J, Levin Y, Geiger B, Martin JF, Tzahor E (2020) ERBB2 drives YAP activation and EMT-like processes during cardiac regeneration. Nat Cell Biol 22(11):1346–1356. 10.1038/s41556-020-00588-4 [PubMed: 33046882]
25. Gordon LI, Burke MA, Singh AT, Prachand S, Lieberman ED, Sun L, Naik TJ, Prasad SV, Ardehali H (2009) Blockade of the erbB2 receptor induces cardiomyocyte death through mitochondrial and reactive oxygen species-dependent pathways. J Biol Chem 284(4):2080–2087. 10.1074/jbc.M804570200 [PubMed: 19017630]
26. Brutsaert DL, Meulemans AL, Sipido KR, Sys SU (1988) Effects of damaging the endocardial surface on the mechanical performance of isolated cardiac muscle. Circ Res 62(2):358–366. 10.1161/01.res.62.2.358 [PubMed: 3338120]
27. Li K, Rouleau JL, Andries LJ, Brutsaert DL (1993) Effect of dysfunctional vascular endothelium on myocardial performance in isolated papillary muscles. Circ Res 72(4):768–777. 10.1161/01.res.72.4.768 [PubMed: 8443868]
28. Del Monte-Nieto G, Ramialison M, Adam AAS, Wu B, Aharonov A, D'Uva G, Bourke LM, Pitulescu ME, Chen H, de la Pompa JL, Shou W, Adams RH, Harten SK, Tzahor E, Zhou B, Harvey RP (2018) Control of cardiac jelly dynamics by NOTCH1 and NRG1 defines the building plan for trabeculation. Nature 557(7705):439–445. 10.1038/s41586-018-0110-6 [PubMed: 29743679]
29. Lemmens K, Doggen K, De Keulenaer GW (2011) Activation of the neuregulin/ErbB system during physiological ventricular remodeling in pregnancy. Am J Physiol Heart Circ Physiol 300(3):H931–H942. 10.1152/ajpheart.00385.2010 [PubMed: 21186272]
30. Kuramochi Y, Cote GM, Guo X, Lebrasseur NK, Cui L, Liao R, Sawyer DB (2004) Cardiac endothelial cells regulate reactive oxygen species-induced cardiomyocyte apoptosis through neuregulin-1beta/erbB4 signaling. J Biol Chem 279(49):51141–51147. 10.1074/jbc.M408662200 [PubMed: 15385548]
31. Cai MX, Shi XC, Chen T, Tan ZN, Lin QQ, Du SJ, Tian ZJ (2016) Exercise training activates neuregulin 1/ErbB signaling and promotes cardiac repair in a rat myocardial infarction model. Life Sci 149:1–9. 10.1016/j.lfs.2016.02.055 [PubMed: 26892146]
32. Lesman A, Habib M, Caspi O, Gepstein A, Arbel G, Levenberg S, Gepstein L (2010) Transplantation of a tissue-engineered human vascularized cardiac muscle. Tissue Eng Part A 16(1):115–125. 10.1089/ten.TEA.2009.0130 [PubMed: 19642856]
33. Chong JJ, Yang X, Don CW, Minami E, Liu YW, Weyers JJ, Mahoney WM, Van Biber B, Cook SM, Palpant NJ, Gantz JA, Fugate JA, Muskheli V, Gough GM, Vogel KW, Astley CA, Hotchkiss CE, Baldessari A, Pabon L, Reinecke H, Gill EA, Nelson V, Kiem HP, Laflamme MA, Murry CE (2014) Human embryonic-stem-cell-derived cardiomyocytes regenerate non-human primate hearts. Nature 510(7504):273–277. 10.1038/nature13233 [PubMed: 24776797]

34. Gao L, Gregorich ZR, Zhu W, Mattapally S, Oduk Y, Lou X, Kannappan R, Borovjagin AV, Walcott GP, Pollard AE, Fast VG, Hu X, Lloyd SG, Ge Y, Zhang J (2018) Large cardiac muscle patches engineered from human induced-pluripotent stem cell-derived cardiac cells improve recovery from myocardial infarction in swine. Circulation 137(16):1712–1730. 10.1161/CIRCULATIONAHA.117.030785 [PubMed: 29233823]
35. Burridge PW, Li YF, Matsa E, Wu H, Ong SG, Sharma A, Holm-strom A, Chang AC, Coronado MJ, Ebert AD, Knowles JW, Telli ML, Witteles RM, Blau HM, Bernstein D, Altman RB, Wu JC (2016) Human induced pluripotent stem cell-derived cardiomyocytes recapitulate the predilection of breast cancer patients to doxorubicin-induced cardiotoxicity. Nat Med 22(5):547–556. 10.1038/nm.4087 [PubMed: 27089514]
36. Voges HK, Mills RJ, Elliott DA, Parton RG, Porrello ER, Hudson JE (2017) Development of a human cardiac organoid injury model reveals innate regenerative potential. Development 144(6):1118–1127. 10.1242/dev.143966 [PubMed: 28174241]
37. Ye L, Chang YH, Xiong Q, Zhang P, Zhang L, Somasundaram P, Lepley M, Swingen C, Su L, Wendel JS, Guo J, Jang A, Rosen-bush D, Greder L, Dutton JR, Zhang J, Kamp TJ, Kaufman DS, Ge Y, Zhang J (2014) Cardiac repair in a porcine model of acute myocardial infarction with human induced pluripotent stem cell-derived cardiovascular cells. Cell Stem Cell 15(6):750–761. 10.1016/j.stem.2014.11.009 [PubMed: 25479750]
38. Huang L, Hou D, Thompson MA, Baysden SE, Shelley WC, Ingram DA, March KL, Yoder MC (2007) Acute myocardial infarction in swine rapidly and selectively releases highly proliferative endothelial colony forming cells (ECFCs) into circulation. Cell Transplant 16(9):887–897. 10.3727/096368907783338181 [PubMed: 18293887]
39. Massa M, Rosti V, Ferrario M, Campanelli R, Ramajoli I, Rosso R, De Ferrari GM, Ferlini M, Goffredo L, Bertoletti A, Klersy C, Pecci A, Moratti R, Tavazzi L (2005) Increased circulating hematopoietic and endothelial progenitor cells in the early phase of acute myocardial infarction. Blood 105(1):199–206. 10.1182/blood-2004-05-1831 [PubMed: 15345590]
40. Massa M, Campanelli R, Bonetti E, Ferrario M, Marinoni B, Rosti V (2009) Rapid and large increase of the frequency of circulating endothelial colony-forming cells (ECFCs) generating late outgrowth endothelial cells in patients with acute myocardial infarction. Exp Hematol 37(1):8–9. 10.1016/j.exphem.2008.09.007 [PubMed: 19013004]
41. Riemenschneider SB, Mattia DJ, Wendel JS, Schaefer JA, Ye L, Guzman PA, Tranquillo RT (2016) Inosculation and perfusion of pre-vascularized tissue patches containing aligned human microvessels after myocardial infarction. Biomaterials 97:51–61. 10.1016/j.biomaterials.2016.04.031 [PubMed: 27162074]
42. Schaefer JA, Guzman PA, Riemenschneider SB, Kamp TJ, Tranquillo RT (2018) A cardiac patch from aligned microvessel and cardiomyocyte patches. J Tissue Eng Regen Med 12(2):546–556. 10.1002/term.2568 [PubMed: 28875579]
43. Melero-Martin JM, Khan ZA, Picard A, Wu X, Paruchuri S, Bischoff J (2007) In vivo vasculogenic potential of human blood-derived endothelial progenitor cells. Blood 109(11):4761–4768. 10.1182/blood-2006-12-062471 [PubMed: 17327403]
44. Smadja DM, Melero-Martin JM, Eikenboom J, Bowman M, Sabatier F, Randi AM (2019) Standardization of methods to quantify and culture endothelial colony-forming cells derived from peripheral blood: position paper from the International Society on Thrombosis and Haemostasis SSC. J Thromb Haemost 17(7):1190–1194. 10.1111/jth.14462 [PubMed: 31119878]
45. Lin Y, Weisdorf DJ, Solovey A, Hebbel RP (2000) Origins of circulating endothelial cells and endothelial outgrowth from blood. J Clin Invest 105(1):71–77. 10.1172/JCI8071 [PubMed: 10619863]
46. Ingram DA, Mead LE, Moore DB, Woodard W, Fenoglio A, Yoder MC (2005) Vessel wall-derived endothelial cells rapidly proliferate because they contain a complete hierarchy of endothelial progenitor cells. Blood 105(7):2783–2786. 10.1182/blood-2004-08-3057 [PubMed: 15585655]
47. Patel J, Seppanen E, Chong MS, Yeo JS, Teo EY, Chan JK, Fisk NM, Khosrotehrani K (2013) Prospective surface marker-based isolation and expansion of fetal endothelial colony-forming cells from human term placenta. Stem Cells Transl Med 2(11):839–847. 10.5966/sctm.2013-0092 [PubMed: 24106336]

48. Lin RZ, Moreno-Luna R, Munoz-Hernandez R, Li D, Jaminet SC, Greene AK, Melero-Martin JM (2013) Human white adipose tissue vasculature contains endothelial colony-forming cells with robust in vivo vasculogenic potential. Angiogenesis 16(4):735–744. 10.1007/s10456-013-9350-0 [PubMed: 23636611]

49. Neumeyer J, Lin RZ, Wang K, Hong X, Hua T, Croteau SE, Neufeld EJ, Melero-Martin JM (2019) Bioengineering hemophilia A-specific microvascular grafts for delivery of full-length factor VIII into the bloodstream. Blood Adv 3(24):4166–4176. 10.1182/bloodadvances.2019000848 [PubMed: 31851760]

50. Lin RZ, Melero-Martin JM (2012) Fibroblast growth factor-2 facilitates rapid anastomosis formation between bioengineered human vascular networks and living vasculature. Methods 56(3):440–451. 10.1016/j.ymeth.2012.01.006 [PubMed: 22326880]

51. Dobin A, Davis CA, Schlesinger F, Drenkow J, Zaleski C, Jha S, Batut P, Chaisson M, Gingeras TR (2013) STAR: ultrafast universal RNA-seq aligner. Bioinformatics 29(1):15–21. 10.1093/bioinformatics/bts635 [PubMed: 23104886]

52. Garcia-Alcalde F, Okonechnikov K, Carbonell J, Cruz LM, Gotz S, Tarazona S, Dopazo J, Meyer TF, Conesa A (2012) Qualimap: evaluating next-generation sequencing alignment data. Bioinformatics 28(20):2678–2679. 10.1093/bioinformatics/bts503 [PubMed: 22914218]

53. Love MI, Huber W, Anders S (2014) Moderated estimation of fold change and dispersion for RNA-seq data with DESeq2. Genome Biol 15(12):550. 10.1186/s13059-014-0550-8 [PubMed: 25516281]

54. Siddiqui MS, Francois M, Fenech MF, Leifert WR (2015) Persistent gammaH2AX: a promising molecular marker of DNA damage and aging. Mutat Res Rev Mutat Res 766:1–19. 10.1016/j.mrrev.2015.07.001 [PubMed: 26596544]

55. Jay SM, Murthy AC, Hawkins JF, Wortzel JR, Steinhauser ML, Alvarez LM, Gannon J, Macrae CA, Griffith LG, Lee RT (2013) An engineered bivalent neuregulin protects against doxorubicin-induced cardiotoxicity with reduced proneoplastic potential. Circulation 128(2):152–161. 10.1161/CIRCULATIONAHA.113.002203 [PubMed: 23757312]

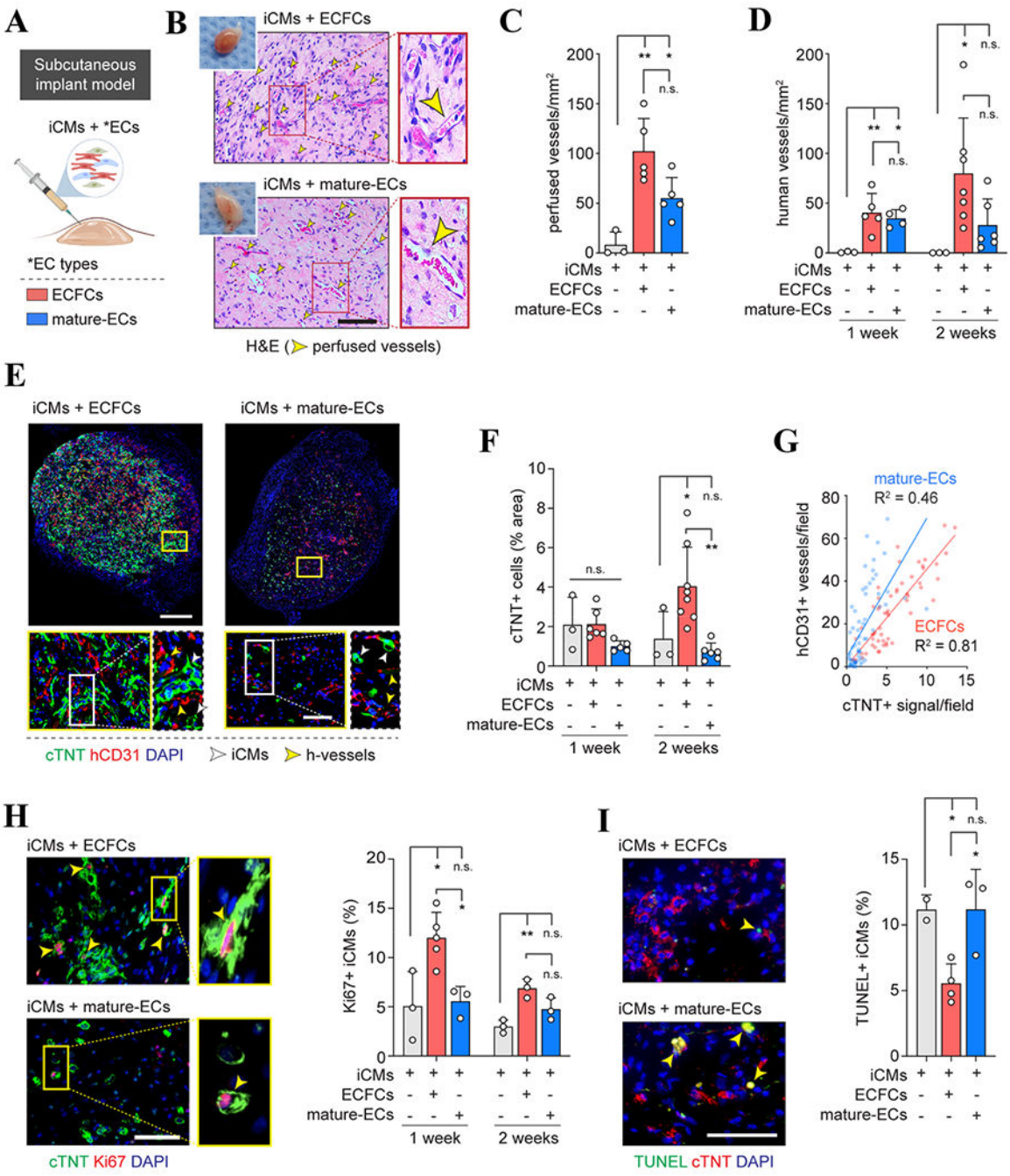

Fig. 1.

ECFCs differentially enhance cardiomyocyte engraftment in a subcutaneous model. **a** Schematic illustration of the in vivo subcutaneous iCM engraftment assay with ECFCs or mature-ECs. **b** Histological (H&E) staining revealing the presence of perfused blood vessels containing erythrocytes (yellow arrowheads) in grafts with either ECFCs or mature-ECs at day 14. Insets are macroscopic views of the explanted grafts. **c** Total perfused microvessel density quantified in explanted grafts at day 14. **d** Human-specific microvessel density quantified in explanted grafts at day 7 and 14. **e** Immunofluorescent staining for human-

specific CD31 (hCD31) and cTNT at day 14. Panels depicted are cross sections of whole implants (upper) and selected regions of the explanted grafts. White arrowheads indicate cTNT + iCMs. Yellow arrowheads indicate hCD31 + vessels. **f** iCM engraftment quantified as the percentage of the total graft area occupied by cTNT + cells at day 7 and 14. **g** Measurements of spatial correlation between the abundance of hCD31 + vessels and cTNT + iCMs within grafts. Lines represent linear correlations for representative grafts and each dot represents a field within the graft at day 14. $n = 5$ grafts for each group. **h** Immunofluorescent staining for proliferation marker Ki67 and cTNT at day 7 (left panel). Percentage of Ki67 + iCMs quantified in grafts at day 7 and 14. **i** Immunofluorescence staining for TUNEL (apoptosis) and cTNT in explanted grafts at day 14. Percentage of TUNEL + iCMs quantified in the indicated groups of grafts. In all quantitative panels, bars represent mean ± s.d. Data is representative of at least 3 independent experiments ($n \geq 3$). *$P < 0.05$, **$P < 0.01$, n.s. = no statistical differences. Scale bars = 500 μm (**e** top), 100 μm (**b**, **e** lower left, **h** left, **i** left)

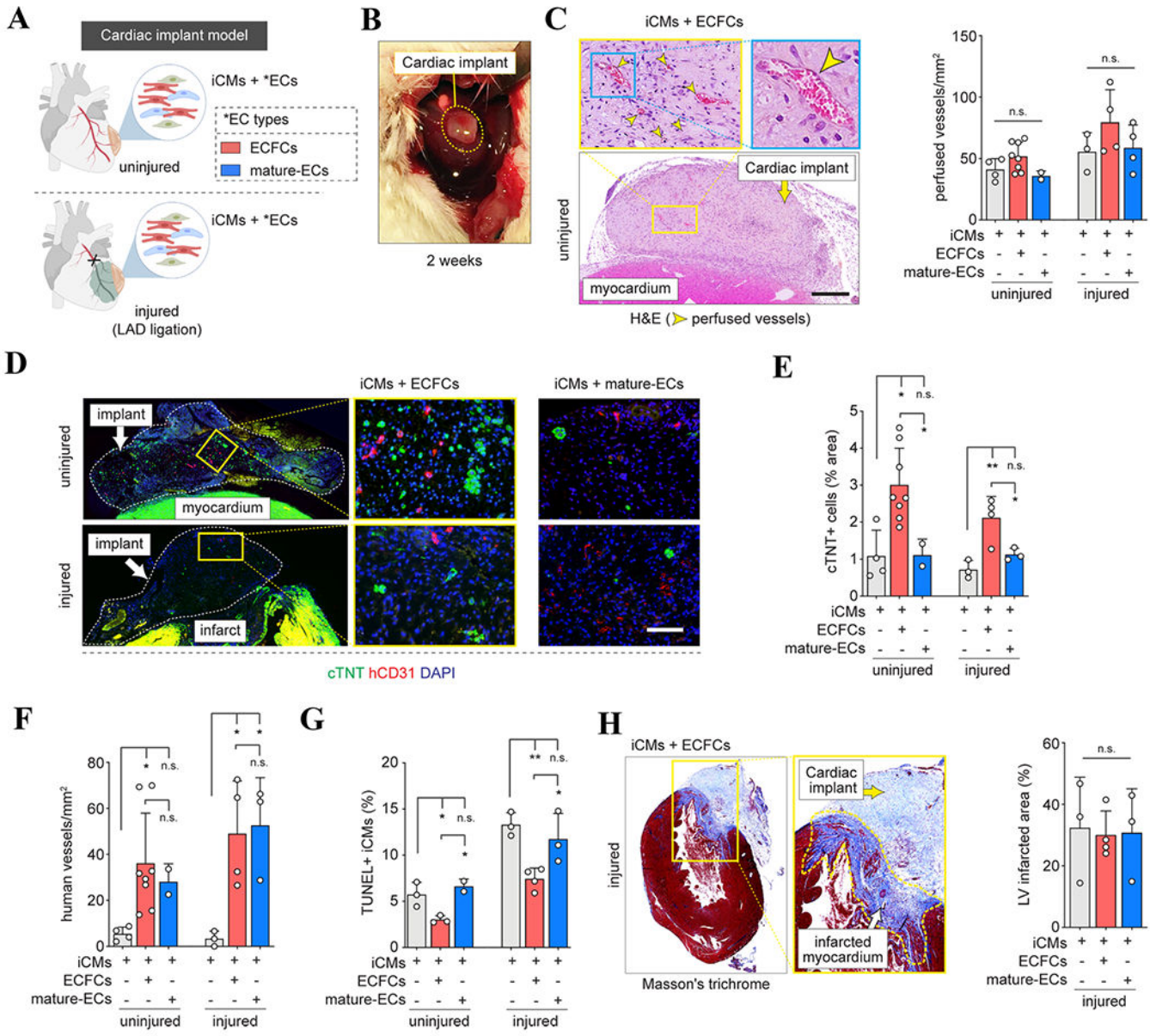

Fig. 2.

ECFCs differentially support iCM engraftment in the myocardium. **a** Schematic illustration of the in vivo cardiomyocyte engraftment models with either ECFCs or mature-ECs in uninjured and injured (permanent LAD ligation) hearts. **b** Representative image of cardiac graft 2 weeks following implantation onto the myocardium. **c** Histological (H&E) staining of a representative cardiac graft attached to the murine myocardium at day 14 (left panel). Total perfused microvessel density quantified in explanted grafts. **d** Immunofluorescent staining for human-specific CD31 (hCD31) and cTNT. Panels depicted are cross sections (left) and selected regions of the explanted cardiac grafts. Nuclei were counterstained by DAPI. **e** iCM engraftment quantified as percentage of the total graft area occupied by cTNT + cells. **f** Human-specific microvessel density quantified in explanted grafts at day 14. **g** Immunofluorescence staining for TUNEL and cTNT. Percentage of TUNEL + iCMs

quantified in the indicated groups of grafts. **h** Masson's trichrome staining of a representative cardiac graft attached to the infarcted myocardium (left panel). Infarct size measured as the percentage of total LV area from the Masson's trichrome-stained slides (right panel). In all quantitative panels, bars represent mean ± s.d. *$P < 0.05$, **$P < 0.01$, n.s. = no statistical differences. Scale bars = 500 μm (**c**), 100 μm (**d**)

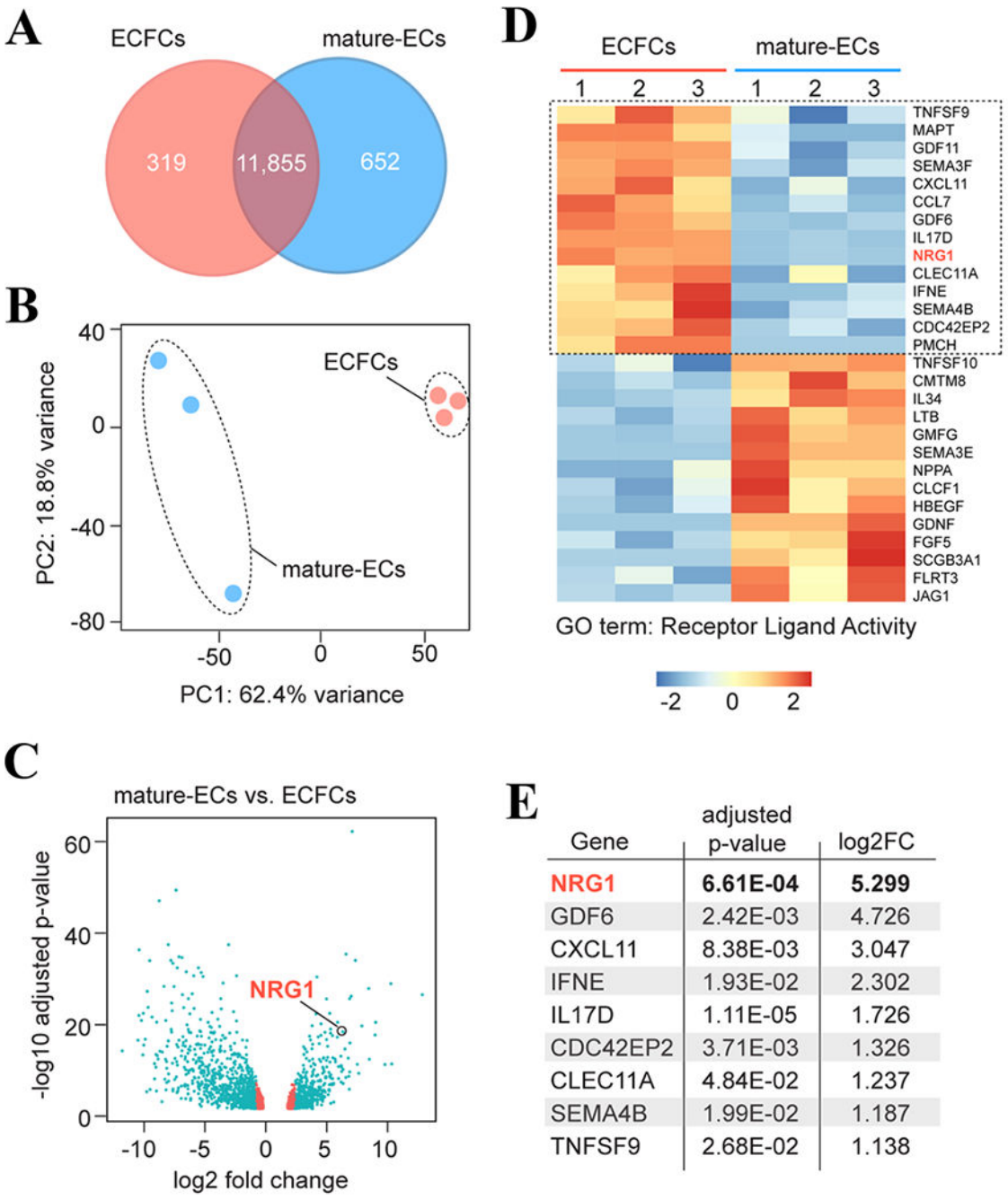

E

Gene	adjusted p-value	log2FC
NRG1	**6.61E-04**	**5.299**
GDF6	2.42E-03	4.726
CXCL11	8.38E-03	3.047
IFNE	1.93E-02	2.302
IL17D	1.11E-05	1.726
CDC42EP2	3.71E-03	1.326
CLEC11A	4.84E-02	1.237
SEMA4B	1.99E-02	1.187
TNFSF9	2.68E-02	1.138

Fig. 3.

Transcriptional analysis of ECFCs and mature-ECs. **a** Venn diagram with the number of differentially expressed genes between ECFCs and mature-ECs. Adjusted *p*-value < 0.05. **b** Genome-wide principal component analysis (PCA) shows distinct clusters that correlated to ECFCs or mature-ECs. **c** Volcano plot for global differentially expressed genes between ECFCs and mature-ECs. Genes with *p*-value < 0.05 and log2 fold change ≥ 0.58 are colored in blue. **d** Heatmap for differentially expressed genes from the GO term: 0048018 (receptor ligand activity). Color bar indicates gene expression in scale. Adjusted *p*-value < 0.05.

Cluster with genes differentially enriched in ECFCs are marked by a dotted box. **e** List of selected genes from GO term: 0048018 sorted by lowest adjusted *p*-value between ECFCs and mature-ECs

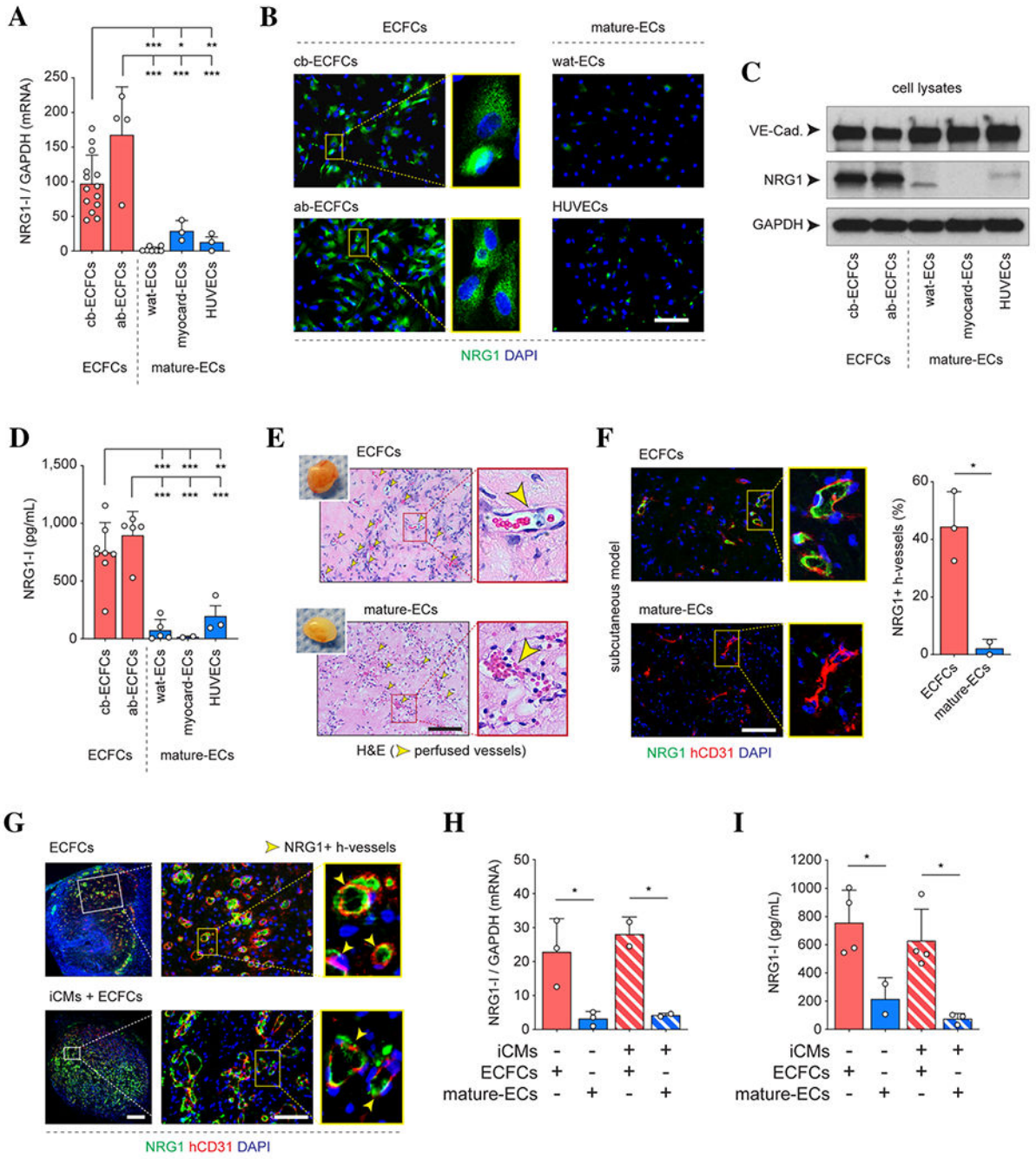

Fig. 4.

Human ECFCs distinctively express and secrete high levels of NRG1. **a** Quantitative real-time PCR analysis of the mRNA level of NRG1 type I (NRG1-I) among different human ECs. Each cell type consisted of cells from at least 2 different individuals. **b** Immunofluorescent staining for NRG1 in different types of ECs. Nuclei were counterstained by DAPI. **c** Western blot analysis for VE-Cadherin and NRG1 protein expression. GAPDH served as the loading control. **d** ELISA analysis of NRG1-I concentration in conditioned medium collected from different types of ECs. Data normalized to per 1×10^6 cells at the

time of conditioned medium collection. **e** In vivo subcutaneous engraftment assay. Grafts containing either ECFCs or mature-ECs and MSCs were subcutaneously implanted into nude mice for 7 days. Insets are macroscopic views of the explanted grafts. Hematoxylin and eosin (H&E) staining revealing the presence of perfused luminal structures containing erythrocytes (yellow arrowheads). **f** Immunofluorescent staining for human-specific CD31 (hCD31) and NRG1 at day 7. The percentage of NRG1 + human vessels quantified. **g** Cardiac grafts containing ECFCs and MSCs were implanted on top of the uninjured heart. Immunofluorescent staining for hCD31 and NRG1 in grafts containing ECFCs with or without iCMs. Yellow arrowheads indicate hCD31 + vessels. **h** Quantitative real-time PCR analysis of NRG1-I expression in hCD31 + cells retrieved from subcutaneous grafts. **i** ELISA analysis of NRG1-I concentration in conditioned media collected from explanted subcutaneous grafts. In all quantitative panels, bars represent mean ± s.d. Each data point represents an independent experiment ($n \geq 3$). *$P < 0.05$, **$P < 0.01$, ***$P < 0.001$, n.s. = no statistical differences. Scale bars = 500 μm (**g** left), 100 μm (**b, e, f, g** right)

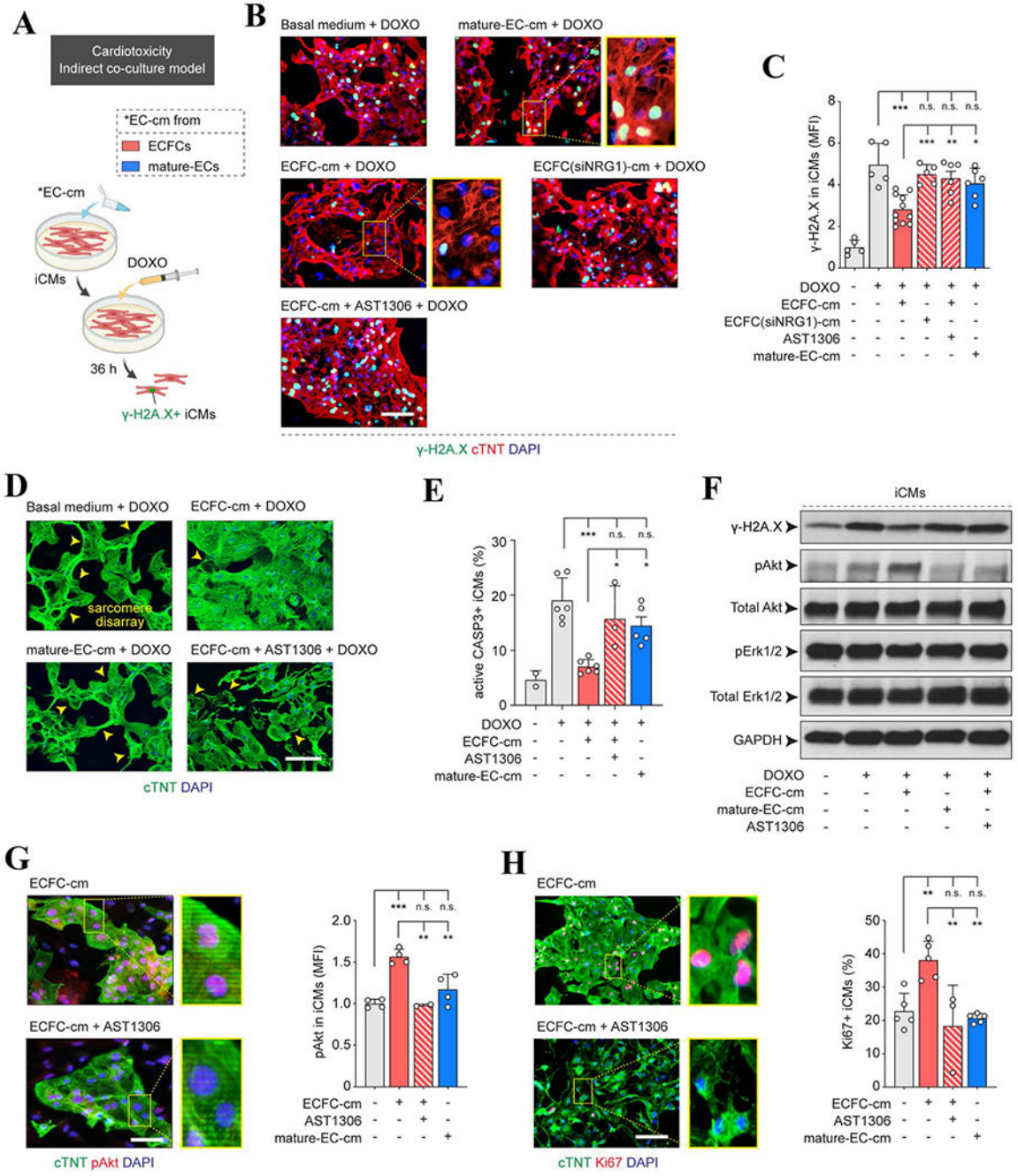

Fig. 5.

Cardioprotective and pro-proliferative ability of ECFCs via NRG1. **a** Schematic illustration of protocol for cardiotoxic drug doxorubicin (DOXO; 2 μM) treatment of cardiomyocyte (iCMs) in the presence or absence of conditioned medium from different ECs (EC-cm). **b** Immunofluorescent staining for DNA damage marker γ-H2A.X and cardiac Troponin T (cTNT) in DOXO-treated iCMs. Nuclei were counterstained by DAPI. **c** Quantification of the mean fluorescence intensity (MFI) of γ-H2A.X within the nuclei of cTNT + iCMs after different treatments. Data normalized to the control group (iCMs treated with vehicle). **d**

Immunofluorescent staining for cTNT in iCMs subjected to indicated treatments. Yellow arrowheads indicate the presence of sarcomere disarray. **e** Percentage of iCMs undergoing apoptosis quantified by the presence of active Caspase-3 72 h after DOXO treatment. **f** Western blot analysis of γ-H2A.X, phosphorylated Akt (pAkt), total Akt, phosphoryl-ated Erk1/2 (pErk1/2), and total Erk1/2 protein expression in iCMs treated with vehicle or DOXO. GAPDH served as the loading control. **g** Immunofluorescent staining for pAkt and cTNT in iCMs cultured under indicated conditions. Quantification (MFI) of pAkt within the nuclei of cTNT + iCMs after different culture conditions. **h** Immunofluorescent staining for Ki67 and cTNT in iCMs cultured in the presence or absence of EC-cm. In all quantitative panels, bars represent mean ± s.d. Data is representative of at least 3 independent experiments ($n \geq 3$). *$P < 0.05$, **$P < 0.01$, ***$P < 0.001$, n.s. = no statistical differences. All scale bars = 100 μm

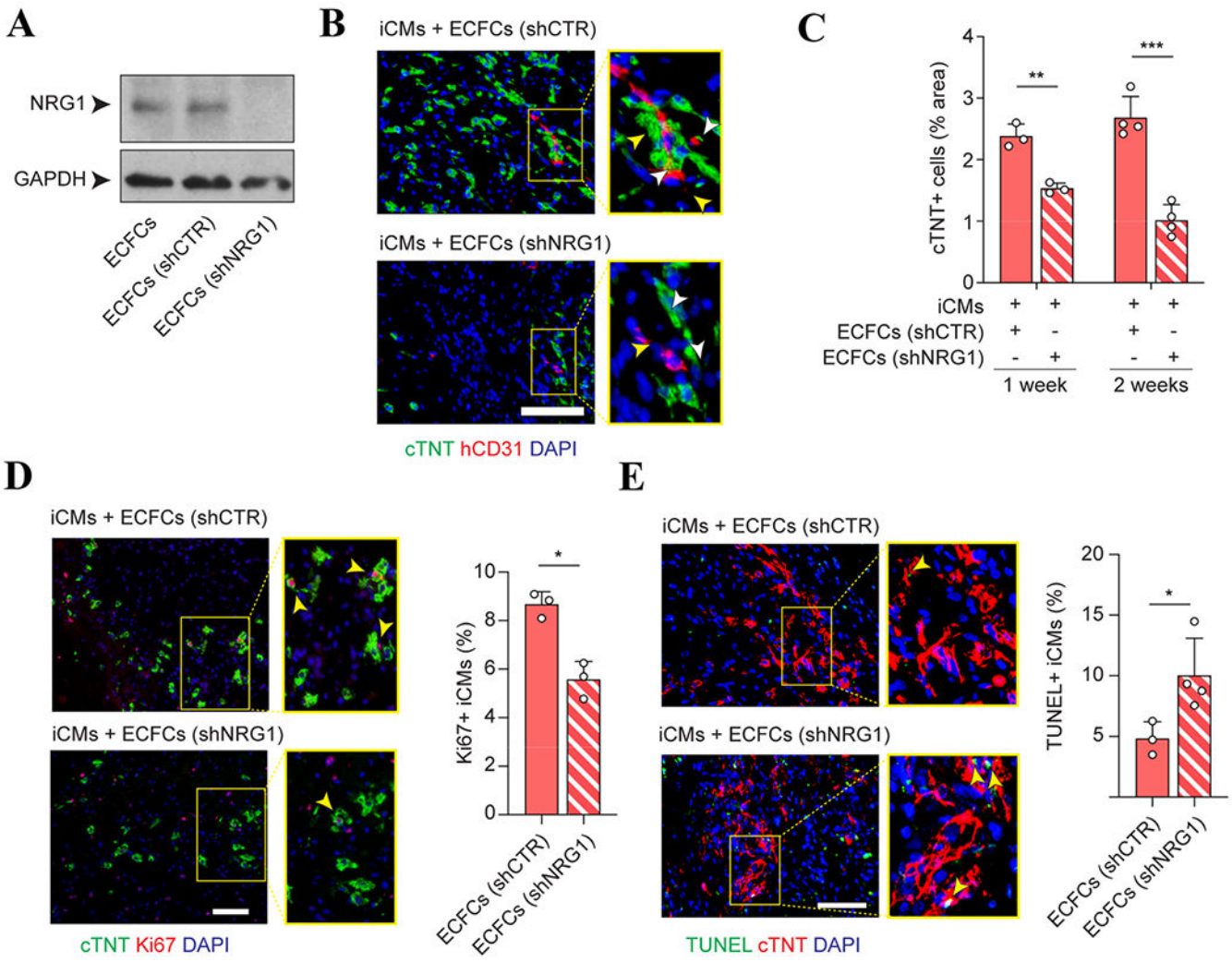

Fig. 6.

ECFCs enhance cardiomyocyte engraftment via NRG1. **a** Western blot analysis confirming efficient knockdown of NRG1 in ECFCs via shRNA (shNRG1). **b** Engraftment of iCMs in the presence of either control ECFCs (shCTR) or ECFCs (shNRG1) lacking NRG1 expression. Immunofluorescent staining for human-specific CD31 (hCD31) and cTNT at day 14. **c** Engraftment of cTNT + iCMs quantified as the percentage of the total graft area. **d** Immunofluorescent staining for Ki67 and cTNT at day 7 (left panel). Percentage of Ki67 + iCMs quantified in the indicated groups of grafts. **e** Immunofluorescence staining for TUNEL (apoptosis) and cTNT in explanted grafts at day 14. Percentage of TUNEL + iCMs was quantified in the indicated groups of grafts. In all quantitative panels, bars represent mean ± s.d. Data is representative of at least 3 independent experiments ($n > 3$). *$P < 0.05$, **$P < 0.01$, ***$P < 0.001$. All scale bars = 100 μm